Review article

Henrik Mäntynen*, Nicklas Anttu, Zhipei Sun and Harri Lipsanen

Single-photon sources with quantum dots in III–V nanowires

https://doi.org/10.1515/nanoph-2019-0007
Received January 8, 2019; revised March 7, 2019; accepted March 7, 2019

Abstract: Single-photon sources are one of the key components in quantum photonics applications. These sources ideally emit a single photon at a time, are highly efficient, and could be integrated in photonic circuits for complex quantum system designs. Various platforms to realize such sources have been actively studied, among which semiconductor quantum dots have been found to be particularly attractive. Furthermore, quantum dots embedded in bottom-up-grown III–V compound semiconductor nanowires have been found to exhibit relatively high performance as well as beneficial flexibility in fabrication and integration. Here, we review fabrication and performance of these nanowire-based quantum sources and compare them to quantum dots in top-down-fabricated designs. The state of the art in single-photon sources with quantum dots in nanowires is discussed. We also present current challenges and possible future research directions.

Keywords: nanowire; single-photon source; quantum dot; III–V semiconductors.

1 Introduction

Quantum photonics employs semiclassical and quantum mechanical properties of photons in the generation, manipulation, and detection of light. Among the various applications for quantum photonics [1], perhaps the most impactful ones are in quantum information science including secure communications via quantum cryptography [2], quantum communication with the realization of the quantum internet [3, 4], and optical quantum computation and simulation to solve classically intractable computational problems [5–7]. All of these applications deal with quantum light fields, including single and entangled photons. Indeed, photons are well suited to operate as decoherence-resistant carriers of quantum information, as they interact only weakly with optically transparent media and can be transmitted by means of free space or fiber optics without interaction among themselves. Photons also have suitable degrees of freedom, like polarization, for the encoding of quantum information [6].

Realizing most of these prospective applications requires efficient single-photon generation, manipulation, and detection. Ideally, all of these functions could be integrated on a chip using nanophotonics fabrication techniques. In addition to well-known linear optical components, highly efficient superconducting nanowire single-photon detectors [8] have emerged that can also be integrated with planar waveguide designs [9]. However, some applications would additionally employ components, such as nontrivial two-qubit quantum gates, which require interaction between two photons in a medium with optical nonlinearity at the single-photon level [1]. Such components are still a major challenge, although, e.g. a two-photon phase shift close to the ideal value of π has been demonstrated for fiber-guided photons [10]. On the other hand, efficient single-photon sources (SPSs) would be immediately useful in applications such as quantum key distribution [12] (using, e.g. the standard BB84 protocol [13]) and linear optical quantum computation [5, 6, 11] (if the emitted single photons are indistinguishable).

Ideally, an SPS deterministically emits exactly a single, indistinguishable photon at a time to a given optical mode. Single-photon generation for quantum photonics has typically been realized by employing (heralded) spontaneous parametric downconversion. However, the spontaneous conversion process is probabilistic, making the sources nondeterministic and hence reducing their usefulness [14, 15]. Increasing the pump intensity improves the generation rate but also increases the chance of generating multiple photons at a time in the output [15]. Another technique for

***Corresponding author: Henrik Mäntynen,** Department of Electronics and Nanoengineering, Aalto University, P.O. Box 13500, FI-00076 Aalto, Finland, e-mail: henrik.mantynen@aalto.fi. https://orcid.org/0000-0002-6468-9594
Nicklas Anttu and Harri Lipsanen: Department of Electronics and Nanoengineering, Aalto University, FI-00076 Aalto, Finland
Zhipei Sun: Department of Electronics and Nanoengineering and QTF Centre of Excellence, Aalto University, FI-00076 Aalto, Finland

obtaining single photons, which is mostly used in current quantum key distribution demonstrations, is to attenuate a laser such that the average power corresponds to less than that of a single photon. Such single-photon emission is also probabilistic and fundamentally limited compared to a high-efficiency true SPS [16].

These shortcomings of the aforementioned SPSs have, in part, motivated the research on alternative SPSs. Significant progress has been made in this area, and single-photon emission has been demonstrated from, e.g. trapped atoms or ions [17, 18], defect sites in various materials [19–22], and semiconductor quantum dots (QDs) [23, 24]. Out of these, semiconductor QDs are among the most promising for on-demand SPSs and can employ a wealth of well-known top-down fabrication techniques and processes from integrated electronics and photonics. For example, this fabrication path offers a promising platform for the realization of entire integrated quantum photonic systems with various semiconductor materials [25, 26].

As a platform, bottom-up-grown semiconductor nanowires can have high aspect ratios with smooth sidewalls and form both axial and radial heterostructures, especially axial QDs, with considerable freedom in choosing the materials and compositions [27–29]. Growth processes of nanowires with embedded QDs are starting to mature and offer a way for fully deterministic positioning of the QDs [30, 31]. Furthermore, nanophotonic structures are often employed to enhance the emission and light extraction from embedded semiconductor QDs, and nanowires can themselves operate as photonic structures that enhance light extraction [32, 33]. Most notably, nanowire growth can be tuned to form a photonic nanoantenna structure [33] for this purpose, which has sparked interest in bottom-up-grown nanowire SPSs as an alternative to top-down-fabricated designs (although the top-down approach currently has attracted more attention).

Here, we review the development and current state of the art in semiconductor SPSs with QDs in bottom-up-grown nanowires and compare them with other semiconductor-QD-based sources obtained via top-down fabrication methods. We will also identify the current challenges with nanowire SPSs and discuss the prospects and possible future research directions. We focus specifically on group III–V QDs, as most of the high-performance SPS demonstrations have been achieved with these materials. SPSs based on colloidal QDs [34] are not considered here. Other recent reviews concerning QD SPSs [16, 24, 35, 36] have not discussed nanowires in detail, and this review will therefore help elucidate the advantages and disadvantages of the bottom-up nanowire growth compared with the top-down approaches to direct future research efforts. Note that, although entanglement plays a major role in many of the aforementioned applications, we focus on single-photon emission; the generation of entangled photon pairs is only briefly mentioned. A recent review on the topic of entangled photon pair generation with semiconductor devices can be found in Ref. [37] and specifically with QDs in Ref. [38].

First, in Section 2, we discuss the characterization of SPSs and the relevant performance metrics, while in Section 3 we introduce the basic principles of single-photon emission from semiconductor QDs. Then, in Section 4, we discuss the emission and extraction enhancement by nanophotonic structures, specifically cavities and nanowires, and in Section 5 we consider the differences in SPS fabrication via top-down methods and bottom-up nanowire growth. In Section 6, we discuss the state of the art in demonstrated performance. Lastly, in Section 7, we discuss the current challenges and prospects for nanowire SPSs, and in Section 8 we present the conclusions.

2 Characterizing single-photon sources

The performance of an SPS can be quantified by considering the following metrics: single-photon purity, indistinguishability of the emitted photons, source efficiency, and source brightness. Single-photon purity is defined as the probability of emitting a single photon instead of multiple photons and is therefore the most fundamental metric. Indistinguishability, on the other hand, concerns the quantum states of successive single photons, with perfect indistinguishability meaning that the photons are emitted to identical quantum states. Many applications require indistinguishability in addition to purity. For example, in linear optical quantum computing, the requirement of indistinguishability is needed to make use of quantum interference between separately generated single photons [6]. Source efficiency states the fraction of applied triggers with which a single photon was collected from the source and is equal to unity in the ideal case. High efficiency is required to obtain deterministic operation. Source brightness is not well defined, but is often used to indicate the maximum rate at which the source can emit single photons (i.e. without degrading the other metrics). However, there exists a discrepancy in the adopted nomenclature such that source efficiency is sometimes referred to as source brightness (see, e.g. Ref. [24]). In the following, we describe briefly the characterization of single-photon purity and indistinguishability,

while a more detailed discussion can be found, e.g. in Ref. [39] and the references therein.

Single-photon purity is typically quantified statistically via the second-order coherence $g^{(2)}(\tau)$, where τ is the time delay between two photons in the emitted light field. At zero time delay, in the case of a single mode and a stationary source, the second-order coherence can be expressed with the photon number operator $\hat{n}(t)$ as [39]

$$g^{(2)}(0)=\frac{\langle \hat{n}(t)(\hat{n}(t)-1)\rangle}{\langle \hat{n}(t)\rangle^2}, \quad (1)$$

where t is time, and the angle brackets denote ensemble average. This also means that the $g^{(2)}(0)$ value is related to the probability $P(n)$ of the source emitting n photons to the mode. In the case of coherent light (photon number probability following Poissonian statistics), $g^{(2)}(\tau)=1$, and for any classical light field, $g^{(2)}(\tau)\geq 1$ [39]. On the other hand, it can be seen from Eq. (1) that a single-photon state yields $g^{(2)}(0)=0$ and an n-photon state yields $g^{(2)}(0)=1-1/n$. Therefore, the condition $g^{(2)}(0)<0.5$ is often considered as the signature of single-photon emission in experiments. Pulsed measurements are not stationary and lead to a modified expression for $g^{(2)}(\tau)$, but the value at zero time delay still equals zero with single photons [39].

Single-photon purity can be experimentally estimated with the so-called Hanbury Brown–Twiss (HBT) interferometer setup [40]. The HBT setup is schematically illustrated in Figure 1A and consists of a beamsplitter, two single-photon detectors, and electronics for coincidence counting and readout. Note that it is also possible to realize the setup with fiber-optic components rather than free-space optics [41]. A single photon passing through the beamsplitter exits in a superposition state of the two output modes. However, the event of detection collapses the superposition and the photon is registered by only one of the detectors. Therefore, single photons result in zero coincidence counts at zero time delay. The second-order

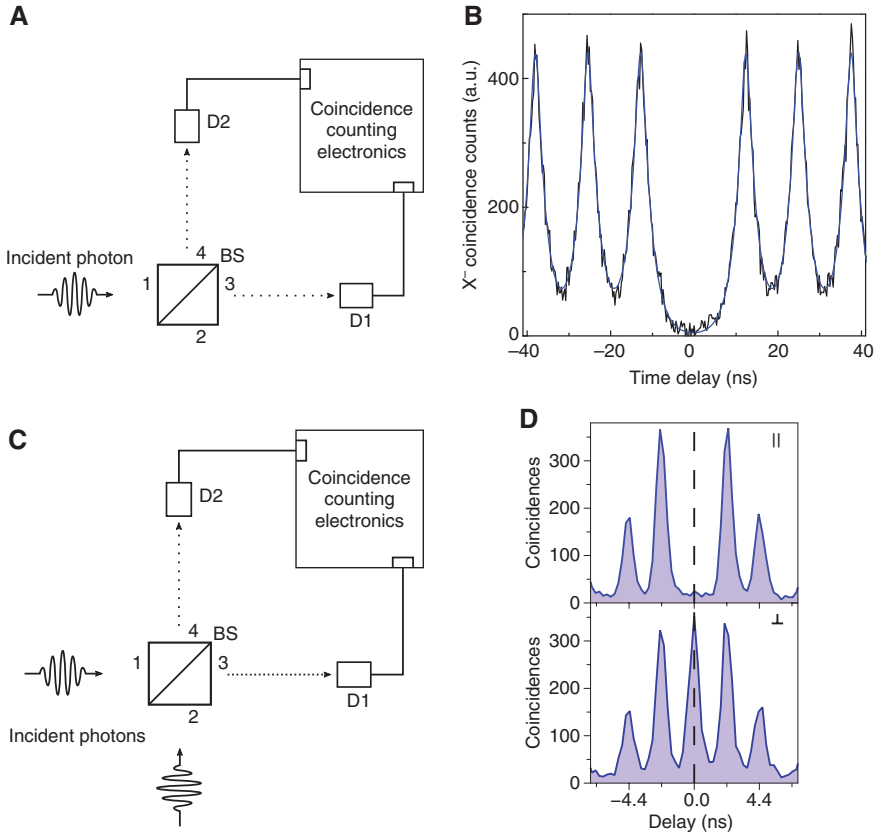

Figure 1: HBT and HOM measurements.
(A) HBT measurement scheme for characterizing single-photon purity. (B) Example HBT measurement result obtained with pulsed excitation of the nanowire SPS reported in Ref. [44] (the blue solid line is a fit to the measured data). (C) HOM measurement scheme for characterizing indistinguishability. (D) Example HOM measurement result obtained with pulsed resonant excitation of the micropillar SPS reported in Ref. [47] and inducing either parallel or perpendicular polarization between the two input modes of the beamsplitter. Figure reprinted with permission from: (B) Ref. [44], 2016 by the American Physical Society; (D) Springer Nature, Nature Photonics, Ref. [47], 2016.

coherence between the beamsplitter outputs $g^{(2)}_{34}(\tau)$ is the same as for the input $g^{(2)}_{11}(\tau)$ and, conveniently, single-photon detectors can be used to obtain $g^{(2)}_{34}(\tau)$ approximately, even if a detector with low efficiency and without photon number resolving capabilities is used (the result can still be accurate if the condition $P(1) \gg P(2) \gg P(n>2)$ is satisfied) [39]. Additionally, coincidence counts with high enough τ values are used for normalization, as $g^{(2)}(\tau) \to 1$ for $\tau \to \infty$, regardless of the type of photon statistics [39]. Experimentally, background light and detector dark counts can lead to false coincidence counts, skewing the statistics, and the raw data is often processed to correct for this (see, e.g. Ref. [42]). Finite time response of the detectors can obscure the $g^{(2)}(0)$ dip and may also be corrected for (see, e.g. Ref. [43]), especially when slow detectors are used. An example HBT measurement result from Ref. [44] is shown in Figure 1B. This result was obtained with pulsed excitation of a high-purity nanowire SPS.

The indistinguishability of two photons can be defined as [39]

$$I(\hat{\rho}_1, \hat{\rho}_2) \equiv 1 - \frac{1}{2} \| \hat{\rho}_1 - \hat{\rho}_2 \|^2, \tag{2}$$

where $\hat{\rho}_1$ and $\hat{\rho}_2$ are the density matrices of the photons, and $\| \hat{\rho}_1 - \hat{\rho}_2 \|^2$ is their operational distance. Ideally, when the density matrices are equal, the two photons are fully indistinguishable with $I(\hat{\rho}_1, \hat{\rho}_2) = 1$. Indistinguishability can be experimentally estimated via the so-called Hong–Ou–Mandel (HOM) interference measurement [45]. The HOM setup is schematically illustrated in Figure 1C and, like the HBT setup, consists of a beamsplitter, two single-photon detectors, and electronics for coincidence counting and readout. Here, photons emitted by an SPS are directed to both the beamsplitter inputs. Typically, the SPS is excited with pairs of trigger pulses, and the resulting train of single-photon pairs is split and directed to the two input modes of the beamsplitter in the HOM setup, with the pulse pair time separation accounted for by the added optical delay for the other input mode (see, e.g. Ref. [46] for more details). An example HOM measurement result from Ref. [47] is shown in Figure 1D. This result was obtained with a high-indistinguishability micropillar cavity SPS.

The idea in the HOM measurement is that, if two photons incident on the two input modes of an ideal 50:50 beamsplitter are in the same pure quantum state and overlap spatially and temporally in the beamsplitter, they will exhibit quantum interference (see, e.g. Ref. [48] for details) and will leave the beamsplitter together in the same output mode. Therefore, there will again be no coincidence counts. Clearly, this requires single-photon states at the inputs, and the HOM measurement is hence also sensitive to the single-photon purity. Purposefully making the photons fully distinguishable, e.g. by removing the overlap via a time delay or by having orthogonal polarizations, allows obtaining the HOM interference visibility as [39]

$$V_{\mathrm{HOM}} = \frac{C_{\mathrm{D}} - C_{\mathrm{I}}}{C_{\mathrm{D}}}, \tag{3}$$

where C_{I} and C_{D} are the coincidence probabilities (or counts in the experiment) with and without the interference, respectively. If the photons are in pure states and the beamsplitter ratio is 50:50, the visibility V_{HOM} equals the indistinguishability as defined in Equation (2) [39]. Some measurement nonidealities, including the residual multiphoton emission probability, an unbalanced beamsplitter, the classical interferometer fringe visibility, and finite detector time response, have also been accounted for when extracting the HOM visibility from raw data [46, 47, 49].

The source efficiency η can usually be divided into the generation efficiency η_{g} and the extraction efficiency η_{ext} as $\eta = \eta_{\mathrm{g}} \eta_{\mathrm{ext}}$ [39]. Generation efficiency states the probability of obtaining emission of a single photon per trigger and depends also on the used excitation (e.g. laser excitation power). Generation efficiency includes both the probability of preparing the emitter in the correct excited state with a trigger and the probability of single-photon emission via the correct radiative transition from that state. The excited state may also decay to the ground state through nonradiative pathways (if these are available), increasing the chance of obtaining zero photons per trigger and hence reducing the efficiency. The extraction efficiency, in turn, states the probability of collecting the emitted photon to an external element, and depends on the outcoupling efficiency from the source and the directionality of the emission from the source. Furthermore, the photon collection is also dependent on the external optical elements (e.g. the numerical aperture of the first lens in free-space collection optics). Unfortunately, there seems to be no clear consensus on the measurement conditions and procedures for SPS efficiency.

Note that, in measurements, single-photon purity and indistinguishability are typically treated as static, although these can actually be dynamically dependent on the excitation and the environment [50]. Single-photon emitters may also exhibit temporary (blinking) or permanent (bleaching) loss of emission under continuous optical excitation, although this is typically a larger concern for colloidal semiconductor QDs [51] than QDs embedded in bulk as discussed here. Furthermore, different measurement

conditions can significantly affect the single-photon emission metrics. For example, resonant excitation of QD SPSs can improve both purity [52] and indistinguishability [47] compared to nonresonant excitation. Additionally, high-efficiency and low-dark-count-rate detectors (e.g. superconducting nanowire single-photon detectors) are required to measure high purity without applying corrections to the obtained result [52]. Therefore, comparing SPS measurement results may not be fair if the measurement conditions differ too much.

3 Single-photon emission from a semiconductor quantum dot

Single-photon emission from a semiconductor QD is based on radiative transitions between the discrete energy levels in the conduction and valence bands. These discrete levels are the result of three-dimensional quantum confinement of the carriers when the QD material has a bandgap smaller than that of the host semiconductor (with type I band alignment such that both electrons and holes are confined in the QD). A short discussion on the fundamental aspects of single-photon emission from semiconductor QDs is given in the following, while a more comprehensive review on the topic of excited states and single-photon emission in QDs can be found in Ref. [35].

Considering the lowest discrete energy levels forming in the conduction and valence bands of the QD (for electrons and holes, respectively), there are only a limited number of excited configurations. Each discrete energy level can support at most two electrons (or holes) with opposite spins due to the Pauli exclusion principle. Furthermore, the small spatial scale of the QD localizes the electrons and holes such that Coulomb interactions lead to the formation of excitons rather than independent electrons and holes. Note that the discrete energy levels in a QD are also referred to as s-shell, p-shell, and so on, following the notation of atomic energy levels. The different charge configurations of the s-shell are then biexciton $|XX\rangle$, charged excitons $|X^{\pm}\rangle$, exciton $|X\rangle$, charged ground states $|g^{\pm}\rangle$, and ground state $|g\rangle$. These configurations are illustrated in Figure 2.

Depending on the spin states, the exciton $|X\rangle$ may or may not have an allowed optical recombination transition (bright and dark state, respectively) [35]. The biexciton $|XX\rangle$, on the other hand, may only form in one way and recombine in two steps emitting two photons. However, the photons will have different energies corresponding to the biexciton binding energy [53]. Similarly, the added interaction in the charged exciton states $|X^{+}\rangle$ and $|X^{-}\rangle$ leads to different emission energies. Furthermore, a radiative transition from an exciton and the corresponding transition from a multi-exciton configuration have different energies due to the effect of the interaction. Therefore, single-photon emission from a chosen transition can be extracted by filtering in energy [54]. The dipole-allowed transitions between these states and the ground state are strongly influenced by the orientation of the natural quantization axis of the QD (typically given by the small height in the vertical direction), leading to transition dipoles perpendicular to this axis [55].

Pure single-photon emission can thus be obtained by exciting the QD and spectrally filtering the emission such that only the photon from, e.g. the radiative recombination $|X\rangle \rightarrow |g\rangle$, is extracted. Such narrow-band spectral filtering is

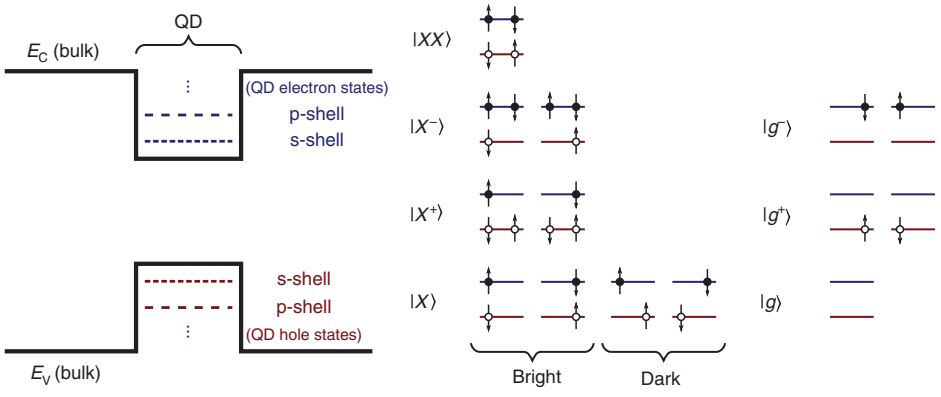

Figure 2: QD states.
Schematic energy band diagram (conduction band E_C and valence band E_V) for a QD embedded in a bulk host semiconductor (left) with possible exciton configurations (exciton $|X\rangle$, charged excitons $|X^{\pm}\rangle$, and biexciton $|XX\rangle$) of the s-shell discrete energy levels (middle) and ground states (charged $|g^{\pm}\rangle$ and neutral $|g\rangle$) corresponding to recombination of the excitons (right). Filled and empty circles represent electrons in conduction band and holes in valence band, respectively. Arrows represent the spin state (up or down).

also possible in integrated solutions [56]. With nonresonant excitation, electrons and holes are generated across the bandgap of the bulk host semiconductor embedding the QD and will diffuse to the QD and relax to the lower energy levels. In order to avoid re-excitation of the QD during a single excitation pulse (i.e. to avoid multiple single-photon extraction per pulse), decay of the generated carrier population in the host semiconductor should occur significantly faster than the radiative recombination in the QD [50].

On the other hand, resonant excitation may be used to directly excite the $|X\rangle$ state, thus reducing the chance of re-excitation and improving the $g^{(2)}(0)$ value. However, it is then necessary to employ additional measures (e.g. a cross-polarization scheme) to reject the scattered excitation laser light [57–59]. Alternatively, the (quasi) resonant excitation may target the next lowest energy levels (p-shell) [60]. Even with resonant excitation, there is a finite chance for QD re-excitation within a single excitation pulse [61]. It is also possible to use resonant two-photon excitation of the $|XX\rangle$ configuration and extract the emission from the $|XX\rangle \rightarrow |X\rangle$ transition by spectral filtering [52, 61]. The benefit of the resonant two-photon excitation is that the QD re-excitation probability is strongly suppressed and that the laser energy is tuned to half of the $|XX\rangle$ state energy and is hence sufficiently far away from the emission wavelength for efficient filtering.

Note that, with the biexciton, it is also possible to obtain a polarization-entangled photon pair [62] via the so-called biexciton–exciton radiative cascade [63]. Due to electron–hole exchange interactions, there is fine-structure splitting (FSS) between the energies of the two bright exciton states with opposing spins [64]. However, if the FSS is small enough, the cascade pair of photons can actually be emitted to a polarization-entangled state. For example, a small FSS can be a result of the QD structure [65] or of tuning with an electric field [66]. Therefore, semiconductor QDs can be used as sources of entangled photon pairs, e.g. with resonant two-photon excitation of the biexciton state [67, 68].

In practice, coupling of the QD emitter with its solid-state environment limits the single-photon purity and indistinguishability. For example, interactions of excitons with phonons causes broadening of the zero-phonon line and the appearance of phonon sidebands [69, 70]. This thermal broadening can lead to spectral contamination from transitions involving different exciton configurations and hence reduced single-photon purity [71]. Cryogenic operation temperatures are often employed to avoid the thermal broadening, although room-temperature SPSs would be preferred for practical reasons. In fact, selecting materials with large band-offsets and fabricating smaller size QDs can increase quantum confinement and Coulomb interaction, leading to larger energy separation between the different excited states. With such materials and small QDs, spectral contamination from other excited states could be significantly reduced to allow single-photon emission even at room temperature [31, 72].

Even with pure single-photon emission, indistinguishability may be limited because of dephasing. First, the emission line broadening due to inelastic exciton–phonon interactions also leads to loss of coherence, and elastic interactions are a source of pure dephasing [69, 73–75]. It was even proposed in Ref. [76] that coupling to phonons ultimately limits the simultaneously achievable indistinguishability and efficiency. In addition to phonons, the QD environment may contain charge traps with a fluctuating charge state generating a fluctuating electric field at the QD, and randomly oriented nuclear spins generating a fluctuating magnetic field, both of which can lead to dephasing [77]. At time scales longer than the exciton radiative lifetime, the electric and magnetic fields generated by the fluctuating charge and spin environment also lead to variation in the energy of the photons emitted (variation in the radiative transition energy) at different times and hence reduced indistinguishability with a large number of consecutive single photons [77, 78]. Note that charge fluctuations in the QD environment causing this spectral diffusion can be due to the effect of nonresonant optical excitation and temperature (phonons) [79–82]. Employing resonant excitation of the QD can, therefore, lead to considerably reduced spectral diffusion [80]. Additionally, the QD emitter could couple to mechanical modes of the SPS structure via strain, also leading to spectral diffusion and reduced indistinguishability [83]. Indistinguishability can be improved by suppressing the effects of the environment, including employing cryogenic temperatures to reduce the phonon population and controlling the charge or spin environment with an applied electric field [47] or additional optical excitation [84]. Alternatively, indistinguishability may be improved by enhancing the spontaneous emission rate (reducing the radiative lifetime) using nanophotonic structures [85].

4 Nanophotonic structures for enhancement of emission and extraction

Semiconductor QDs inside a piece of bulk semiconductor are not good for high-performance SPSs, as the extraction efficiency is severely limited by the lack of directionality in

the QD emission and by the total internal reflection occurring at the semiconductor–air interface (high refractive index contrast leads to a very narrow solid angle within which the emitted light can escape the bulk semiconductor and the extraction is in the order of a few percents for typical III–V semiconductors). The total internal reflection problem could be solved by using, e.g. solid or liquid immersion lenses [86]. However, a more elegant way is to employ nanophotonic structures, as these structures may not only improve the extraction efficiency but also enhance spontaneous emission to a desired optical mode inside the structure or inhibit emission to other modes. Furthermore, nanophotonic structures offer, in principle, the possibility for on-chip integration.

For both extraction efficiency and single-photon indistinguishability, it is highly desirable that an SPS emits to a single, well-defined optical mode. The preference in emission coupling to a desired optical mode within a photonic structure can be expressed by the β-factor [87]

$$\beta = \frac{\Gamma}{\Gamma + \gamma}, \tag{4}$$

where Γ is the spontaneous emission rate to the desired mode supported by the structure, and γ is the spontaneous emission rate into all other modes. The extraction efficiency then further depends on the outcoupling efficiency of photons in the desired mode and the directionality of the outcoupled light field (which in turn affects how well the emitted photons in the mode can be collected).

Various photonic structure designs have been employed for semiconductor QD SPSs, including planar cavities [58, 66], micropillar cavities [47, 84, 88–92], microdisk cavities [93, 94], photonic crystal cavities [95–97] or waveguides [59, 98, 99], and novel photonic structures such as nanotrumpets [100], optical horns [101], and nanowires [33, 44]. An important early demonstration of QD single-photon emission was achieved using a microdisk cavity [93]. So far, cavity structures (especially micropillar cavity structures) have provided the best performance in top-down-fabricated SPSs [47, 52, 92, 102], while bottom-up-grown nanowire SPSs tend to employ the nanoantenna scheme introduced in Ref. [33]. These two types of photonic structures are briefly discussed here, while a more general review on interfacing QD single-photon emission with photonic nanostructures can be found in Ref. [35].

4.1 Cavities

An optical cavity essentially confines the light field to a small volume, giving rise to certain optical modes that are resonant within the cavity. As proposed by Purcell [103], the spontaneous emission from an emitter depends also on the environment or, more specifically, the available optical density of states at the location of the emitter (the so-called Purcell effect). A cavity structure modifies the optical density of states and, when properly designed, results in significant enhancement of the spontaneous emission to the resonant modes. The enhancement (ratio) of spontaneous emission rate to a specific optical mode with a photonic structure compared to the case in the absence of the structure (i.e. just bulk material) is expressed by the Purcell factor F_p of this specific mode [104]. Increasing F_p therefore increases both the single-photon emission rate and the source extraction efficiency (via increasing the β-factor through an increase of Γ in Eq. (4)). Indistinguishability is also simultaneously increased, although only up to reaching the QD–cavity strong coupling regime [75, 76].

An increase in the Purcell factor of the mode can be achieved by increasing the cavity quality factor, but doing so also makes the cavity more frequency-selective, which then necessitates more accurate matching of the cavity resonance with the QD emission wavelength [35]. It is generally difficult to achieve accurate matching directly by design due to various fabrication imperfections. One way to achieve matching post fabrication is to alter the operation temperature, as the QD emission (via the bandgap) and cavity resonance wavelength (via the refractive index) usually have different temperature dependences [105]. However, since increasing the temperature has an adverse effect on indistinguishability, an alternative approach is to use a fixed low temperature and tune the QD emission via the quantum-confined Stark effect by applying an electric field across the QD [106, 107]. On the other hand, the applied electric field reduces the overlap of the electron and hole wave functions, thus reducing the oscillator strength of the transitions and increasing the radiative lifetimes with reduced emission rate [107, 108]. The strength of the applied field, as well as the tuning range, is also limited by the onset of carrier tunneling out from the QD [106–108].

Planar and micropillar cavities are commonly employed in top-down SPSs. Both types of cavities use distributed Bragg reflectors (DBRs) to form the cavity by confining light into it. A DBR consists of a stack of alternating quarter-wavelength-thick layers with different refractive indices, and the reflectivity depends on the number of layers. One of the two DBRs is designed to act as an efficient reflector (reflectivity close to 100% around the cavity resonance wavelength), while the other is designed to be semitransparent in order to extract the light from that side.

The planar cavity structure is simpler and easier to realize, including fabrication of electrical contacts for tuning with an electric field. The top contact layer can also be used as an aperture to isolate a single QD [66]. Unfortunately, the extraction efficiency with planar cavity structures is rather poor (e.g. around 1.3% overall collection efficiency in Ref. [58]). With micropillar cavities, the pillar structure offers additional light confinement in the radial direction and improved extraction efficiency (e.g. around 65% in Ref. [84]). Basically, a diode structure with either annular top contact pads [90] or top contacts to surrounding structures connected via sidewall wires [47, 91] can be employed for the electric field tuning in micropillar cavities.

Photonic crystal cavities have also been employed [95–97]. In short, these are defined by a defect in the otherwise periodic structure, and the light confinement to this defect region is given by the photonic bandgap that prevents light propagation in the periodic region (assuming that the photonic crystal is designed such that the QD emission wavelength is within the range of the photonic bandgap). Photonic crystal cavities offer light confinement in very small volumes and both enhancement of emission to the cavity mode and inhibition of emission to radiation modes [35]. Alternatively, QDs may be embedded inside photonic crystal waveguides (extended defects in the periodic structure) for in-plane emission and routing of photons with a near-unity β-factor [98, 109]. The light may also be extracted from photonic crystal waveguides using outcoupling structures [98, 109] or even direct coupling to an optical fiber [99].

4.2 Nanowire nanoantenna

Nanowires can embed QDs along their axis and act as waveguides with highly efficient, directional outcoupling after proper design. The idea of using QDs obtained via axial nanowire growth as SPSs was mentioned, e.g. in Ref. [110] in 2002, and likely even before that, while some of the early experimental realizations of this idea include Ref. [111] in 2005 and Ref. [112] in 2010. The nanowires in Ref. [111] exhibited $g^{(2)}(0) < 0.5$, demonstrating operation as SPSs. In Ref. [112], improved single-photon emission ($g^{(2)}(0) = 0.12$) as well as biexciton–exciton radiative cascade was obtained. Common to these two examples is that the nanowires were still used as such without further engineering effort to improve the emission or light extraction.

In 2009, a nanowire structure working as a nanoantenna, which greatly improves the source efficiency, was proposed in Ref. [33]. The nanoantenna design constitutes three different factors as illustrated in Figure 3.

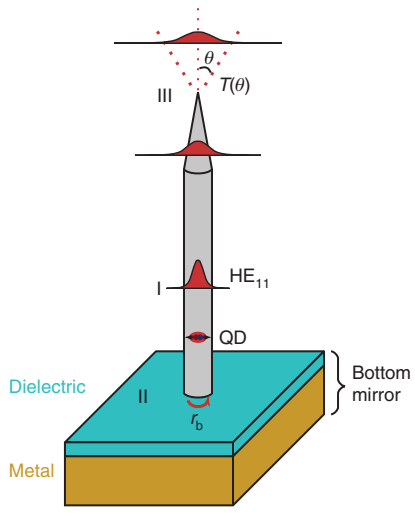

Figure 3: Schematic nanowire nanoantenna SPS design. The nanoantenna design includes (I) optimized nanowire diameter for funneling the QD emission into the guided HE_{11} mode, (II) bottom mirror to reflect the downward emitted photons (modal reflection coefficient r_b), and (III) tapered nanowire tip to adiabatically expand the guided mode outside the nanowire for minimized backreflection (transmission $T(\theta)$ into an upward cone with angle θ).

First, the ratio of the nanowire diameter to the emission wavelength is optimized such that there is only one guided mode (i.e. the fundamental HE_{11} mode) available along the nanowire axis into which the emission can couple. Furthermore, the diameter-to-wavelength ratio is chosen to maximize the funneling of emission into that mode by suppression of coupling to the continuum of radiation modes. Second, the HE_{11} mode may travel toward the substrate (away from the light collection direction) but can be directed back by using a properly designed bottom mirror (e.g. a dielectric/metal mirror [113]). This design also requires tuning the QD-to-mirror distance in order to obtain an antinode in the electric field at the QD, so that the reflection enhances maximally the emission into the HE_{11} mode (i.e. enhances the Purcell factor of the mode). Third, if the nanowire tip is fabricated to have a conical taper toward the top, the HE_{11} mode will be adiabatically expanded outside the nanowire. Then, the mode couples out into a low-numerical-aperture emission lobe. Therefore, the extraction efficiency becomes enhanced as a result of the minimized reflection of the HE_{11} mode back to the nanowire. In addition, the low-numerical-aperture emission lobe from the tapered tip makes the collimation easier (compared to the case of a flat nanowire tip), facilitating photon collection with external optics of limited numerical aperture. To some extent, these features had already been discussed earlier, e.g. emission to guided modes in Ref. [32], bottom mirror

designs and performance in Ref. [114], and the tapered tip in Ref. [115].

High β-factor values above 0.9 are achievable with the nanowire nanoantenna design [33, 104]. The high β-factor values are additionally obtained over a relatively broad wavelength band ($\Delta\lambda/\lambda = 0.26$ [33, 116]) compared to the narrow resonances in cavities [33], which gives more tolerance to fabrication imperfections. Such a broadband response also facilitates an easier use of quasi-resonant excitation or resonant two-photon excitation and generation of entangled photon pairs with different wavelengths, both of which are more difficult to match with cavity modes. On the other hand, this broadband operation may also limit the ultimate trade-off between single-photon indistinguishability and efficiency (see the discussion in Ref. [76]). If constructive interference is assumed for the field reflected by the bottom mirror at the emitter, and multiple reflections inside the nanoantenna are not taken into account (i.e. if we assume that the reflection of the HE_{11} mode at the nanowire tip is negligible), the extraction efficiency for the nanowire antenna may be written as [33]

$$\eta_{\mathrm{ext}} = T(\theta)\frac{\beta(1+|r_{\mathrm{b}}|)^2}{2(1+\beta|r_{\mathrm{b}}|)}, \tag{5}$$

where $T(\theta)$ is the tip transmission into an upward cone with angle θ and r_{b} is the reflection coefficient for the guided mode at the bottom mirror. At the optimized condition of $T(\theta)\approx 1$ and $|r_{\mathrm{b}}|\approx 1$, Eq. (5) further simplifies to $\eta = 2\beta/(1+\beta)$. Theoretically, the extraction efficiency could then go as high as around 95% [33]. This, however, does not take into account any loss mechanisms such as scattering due to sidewall roughness. A more detailed inspection of the nanowire nanoantenna design can be found in the review in Ref. [116].

5 Single-photon source fabrication

Both top-down-fabricated and bottom-up-grown SPSs most often employ vapor-phase epitaxial crystal growth methods including metal-organic vapor phase epitaxy (MOVPE), molecular beam epitaxy (MBE), and chemical beam epitaxy (CBE). The main difference, however, is in how the device structures are obtained: in top-down fabrication, patterning and etching are used to selectively remove grown material, while in bottom-up nanowire fabrication, patterning can be used to achieve selective growth of material. Nanoscale patterning is typically achieved via electron beam lithography (see, e.g. Ref. [117]) or nanoimprint lithography (see, e.g. Ref. [118]), although optical lithography may certainly be used for patterning micrometer-scale pillars and aperture openings. Both top-down and bottom-up nanowire approaches have benefits and shortcomings, which are briefly discussed in the following.

5.1 Top-down-fabricated sources

Generally, the top-down fabrication approach for SPSs is based on epitaxial growth of materials combined with deposition of other materials (e.g. for a mask layer) and patterning via lithography and etching. With certain materials, such as GaAs, the epitaxial MBE thin-film growth has been optimized to such a high degree that it is possible to achieve monolayer precision in thickness with high-quality interfaces [25]. This technique is therefore ideally suited for the fabrication of planar cavity structures with DBR stacks. On the other hand, with micropillars and photonic crystals, etching processes unavoidably lead to some sidewall surface roughness in the etched features, which can be problematic. For example, narrower micropillar structures start to suffer from increased losses due to the sidewall roughness [119]. Note that the effect of sidewall roughness is pronounced by cavities, within which the light typically circulates a large number of times before outcoupling, giving increased chance for a scattering event due to the sidewall roughness (at the cavity location). In contrast, in the nanowire nanoantenna SPS, the photon travels the nanowire only once, reducing the impact of sidewall roughness.

The most often employed semiconductor QD fabrication method is the so-called Stranski–Krastanov self-assembled growth mode. In this growth mode, lattice mismatch between the growing layer and the substrate material leads to strain relaxation via random nucleation and growth of island-like formations after first forming a few planar monolayers (the so-called wetting layer) [120]. The grown QD islands can then be capped with epitaxial growth so that they become embedded. The emission energy of such a self-assembled QD island depends on the composition (with ternary or quaternary compounds), size, and strain. To complicate matters, the composition affects the strain via lattice mismatch, and the strain in turn affects the QD size. Furthermore, the emission energy depends on the surrounding host semiconductor material, which determines the strength of the charge carrier confinement in the QD.

An ensemble of self-assembled QDs in a single sample tends to exhibit a distribution of sizes (variation

from island to island) with typical lateral extents around 10–70 nm and heights around 1–10 nm [35]. The density of the dots forming on the substrate can be controlled by varying the growth conditions [121], which is useful, as a low density is required to find single isolated QDs for fabricating SPSs. The QD size distribution can be controlled to some extent as well [122, 123]. However, inter-mixing between the QD and capping materials can take place during the growth, which may further increase the variation in the optical properties of the QDs [25]. The most studied material systems for self-assembled QDs are InAs and InGaAs on GaAs substrates; with these materials it is possible to obtain emission in the spectral range starting from around 850 nm and including the telecom C-band (1530–1565 nm) [25, 124].

The randomness in location and inhomogeneity in the QD ensemble is the biggest drawback of the self-assembly approach, as QDs well separated from other QDs need to be first located and characterized before further processing. Highly accurate positioning of the QD within either a micropillar or photonic crystal cavity is required to obtain good coupling to the cavity mode, and accurate QD positioning is also needed for emission-coupling to the guided mode in a photonic crystal waveguide [35, 125]. It is alternatively possible to, e.g. etch a large array of micropillars in a sample with self-assembled QDs and statistically obtain a few devices with adequate spatial and spectral matching [105]. This approach can be acceptable if only a single or a few operating devices are needed but is unsuitable for large-scale on-chip integration. One approach to locate a suitable QD and align the subsequent patterning is to fabricate markers on the substrate, measure the QD emission with confocal photoluminescence scanning microscopy (or some other technique with sufficient spatial resolution), record the location of QDs (location where the emission shows highest intensity) with respect to the markers, and align the patterning using the markers and known relative coordinates of the QDs. This approach was taken, e.g. in Ref. [125], where sub-10-nm positioning accuracy was achieved. On the other hand, a more convenient in situ optical technique for combined spatially resolved QD emission measurement and far-field lithography was presented in Ref. [126], where a good QD-to-micropillar axis alignment with accuracy of <50 nm could be achieved.

Even with sophisticated in situ characterization and lithography techniques, large-scale integration with self-assembled QDs cannot be judged feasible, as the layout can only be designed after locating suitable QDs and there would be a large number of extra QDs that need to be avoided or removed. Therefore, considerable research efforts have been directed to develop fabrication techniques that provide site-controlled QD growth [127]. Such site-controlled techniques include growth in etched holes [128, 129], growth in etched holes combined with vertical stacking [130, 131], preferential growth on oxide patterns realized by local oxidation nanolithography [132], and directed self-assembled growth on nanotemplates [133]. Site-controlled high-symmetry QDs embedded in pyramid structures grown to etched tetrahedral recesses have even demonstrated entangled photon pair generation [134]. However, further development is still needed in order to obtain a high degree of control and sufficiently high QD quality with these techniques [25, 35, 36].

One example of a state-of-the-art top-down-fabricated micropillar cavity SPS can be found in Ref. [47]. The fabrication process of this SPS can be roughly divided to the following steps: (i) high-quality MBE growth of a planar n–i–p doped diode structure with GaAs/$Al_{0.9}Ga_{0.1}As$ DBR stacks and self-assembled InGaAs QDs in the intrinsic region; (ii) combined characterization and lithography technique for locating the QDs and patterning an etch mask; (iii) etching of the micropillar and connected mesa structures, and (iv) forming electric contacts to the substrate and the mesa structure for electrical field tuning (field across the micropillar diode with embedded QDs).

5.2 Bottom-up-grown nanowire sources

Bottom-up growth of semiconductor nanowires offers a way to fabricate high-aspect-ratio structures with smooth sidewall surfaces and both axial and radial heterostructures or doping profiles. Due to the nanowire geometry, stress resulting from lattice mismatch is more efficiently accommodated via strain relaxation in the radial direction without the formation of dislocations [135–137]. Therefore, heterostructures in nanowires can employ a wider variety of materials and compositions than in planar configurations where epitaxial thin-film growth requires lattice matching and the aforementioned Stranski–Krastanov QD growth requires suitable lattice mismatch.

There are two distinct growth modes by which nanowires can be realized: vapor–liquid–solid (VLS) and selective-area epitaxy (SAE). In general, III–V nanowires can grow either epitaxially or non-epitaxially and tend to prefer the [111] crystalline orientation [138] with polytypism in the crystal structure between the zincblende and wurtzite structures (unlike bulk III–V materials which tend to only exhibit the zincblende structure, except for the nitrides) [139]. Note that the difference in the two growth modes is mainly in the axial nanowire growth,

whereas the radial vapor–solid growth is similar for both modes. Both growth modes allow forming heterostructure QDs.

The VLS nanowire growth, in short, is mediated by a metallic droplet that is assumed to be in liquid phase and collects the growth species (at least group III) introduced in vapor phase, leading to nucleation and solid crystal growth below the droplet. The growing nanowire then lifts up the droplet that sits at the tip of the nanowire. The VLS growth is schematically illustrated in Figure 4A. The metallic droplet material can either be one of the group III growth species (which is often called self-catalyzed or self-assisted growth) [140] or a foreign material, among which Au is the most common and well known [141]. Nanoscale patterning of openings in a mask layer for self-assisted growth, or Au disks for Au-assisted growth (with or without a mask), may be used to define the nanowire growth sites [30, 117, 142].

The VLS growth mode was originally introduced by Wagner and Ellis [143], who considered the growth of Si "whiskers" with the aid of Au droplets. Since then, more research was conducted on Si [144], after which the focus shifted to mainly III–V materials such as GaAs, GaP, InP, InAs, and their ternaries [145–148]. In the past couple of decades, considerable research effort has been made to understand the effect of various growth conditions and substrate preparations for VLS nanowire growth [149–152]. It has become possible to obtain nanowires of high crystal quality [139], to control the crystal phase [139, 153], to switch between axial VLS growth and radial vapor–solid growth [154], to dope the nanowires during growth [155], and to obtain axial and radial heterostructures [28, 30, 110, 156]. Despite the significant progress that has been made, the detailed growth mechanism is still not fully understood and research in this area is going on [27, 151].

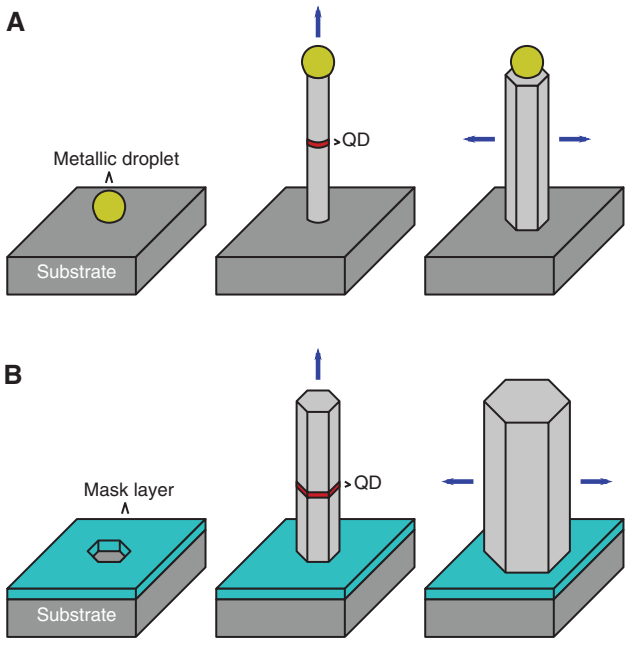

Figure 4: Schematic illustration of the nanowire growth modes. (A) VLS growth mode where axial growth is mediated by a metallic droplet (typically Au). (B) SAE growth mode where growth takes place at an opening in a mask layer. Radial growth takes place via direct vapor—solid growth in both modes. The growth direction (axial or radial) is indicated with blue arrows, and heterostructure insertions (QDs) are indicated with red color. The ideal case is depicted here, where axial and radial growth can be independently controlled to obtain the desired nanowire geometry.

SAE growth, on the other hand, is direct vapor–solid growth and is based on growth mask layers and differences in the nucleation and crystal growth on different crystal facets due to differences in surface energies [157]. Openings in the growth mask exposing the underlying substrate define the locations where nanowires start to grow, and for axial growth when the substrate surface is a {111} plane, the growth conditions are selected such that the $\{\bar{1}10\}$ facets have significantly lower growth rate than the {111} facets. Then, $\{\bar{1}10\}$ sidewall facets emerge and the growing crystal assumes a vertical nanowire shape with hexagonal cross-section. Ideally, the radial growth can be fully suppressed during axial growth, and the nanowire diameter is set by the size of the mask opening. The SAE growth is schematically illustrated in Figure 4B. Note that, unlike in the figure, the mask opening does not need to be a hexagon and the nanowire may grow laterally wider than the opening to assume the hexagonal shape (even in the case of negligible radial growth rate afterward).

Typical III–V materials for SAE nanowire growth include GaAs [157, 158], InP [159], InAs [160], and some ternary compounds [158]. Since patterning is already a part of the process, regular arrays with a square or hexagonal lattice are typical. As with VLS growth, it is possible to obtain high crystal quality [159], to control the crystal phase [161], to switch between axial and radial growth [29], to dope the nanowires during growth [29], and to obtain axial and radial heterostructures [29, 162]. In principle, SAE growth is simpler than VLS growth, as only two phases, vapor and solid, are involved and no foreign material, such as Au, is present. Still, the growth dynamics are complicated by, e.g. dependence on size and spacing of the mask openings, on the evolving nanowire geometry during the growth, and on the relative supply of group III (or V) constituents in the growth of ternaries [163–165]. Consequently, understanding the subtleties

and obtaining a high degree of control in nanowire SAE growth is a challenge.

Conceptually, obtaining QDs in nanowires with either growth mode is simple: new materials are briefly introduced during the axial nanowire growth such that a section of the lower bandgap material will be inserted in the growing nanowire. Patterning of the metallic droplets in VLS or the mask openings in SAE defines the lateral position of the nanowire, diameter of the droplets or openings defines the QD diameter, and axial growth times define the QD vertical position and height. Therefore, patterning combined with bottom-up growth offers full control over the positioning and size of the QD. Radial growth may then be used to fully embed the QD inside the nanowire. Alternatively, it is possible to clad the nanowire with an atomic layer deposition (ALD) oxide shell in order to obtain a waveguide structure [166]. However, nanowire heterostructure growth is not trivial in practice. For example, obtaining abrupt interfaces in axial growth (especially with VLS) is difficult due to various memory effects leading to composition gradients [27, 167–169]. In Au-assisted VLS, the solubilities of group V species in the Au droplet are low compared to those of group III [148]. It is therefore generally easier to form axial QDs by switching of the group V material during the growth than by switching group III, which is however still possible [168]. Regardless, a rather impressive level of control in growing QDs in nanowires has been achieved. This control allows, e.g. fabricating pairs of QDs with small enough spacing such that the electronic states become coupled. This coupling was recently demonstrated in Ref. [170], where a coupled QD pair in a nanowire emitted entangled photon triplets via a triexciton triple cascade.

Compared to top-down fabrication, there are some major advantages with the bottom-up nanowire growth for SPS fabrication: wide material compatibility, deterministic fabrication yielding a single QD per nanowire, and natural alignment of the QD to the nanowire waveguide axis. The most researched material system is InAsP QDs in InP nanowires, with which the emission can span the wavelength range starting from around 880 nm and including the telecom C-band [171, 172] (at cryogenic temperatures). For example, an SPS operating at the wavelength 1310 nm (in the telecom O-band) has been demonstrated with this material system [172]. Single-photon emission has also been demonstrated, e.g. around 725 or 765 nm with GaAs QDs in AlGaAs [173, 174], 286 nm with GaN QDs embedded in AlGaN [31], and 468 nm with InGaN QDs (or nanodisks) embedded in GaN [175]. Various III–nitride QDs should overall be able to cover emission from ultraviolet to telecom wavelengths [175]. Furthermore, it is also possible to grow nanowires with basically all these materials on top of Si [174, 176–178], with the prospect of III–V SPS integration with Si photonics. Assuming symmetric radial shell growth, the axial QD becomes embedded exactly on the axis of the nanowire waveguide in one monolithic growth step, quite unlike in the previously discussed top-down fabrication with alignment procedures. Still, the nanowire SPSs may also need to be individually characterized, as the QD emission wavelength may vary from wire to wire due to growth variations.

On the other hand, there is no feasible way to grow nanowires with both axial QDs and DBR stack cavity structures for improved indistinguishability. These two features cannot be simultaneously achieved because thick nanowires are needed for efficient DBR stacks [114], which is incompatible with axial QD growth. Furthermore, nanowire growth processes are in general not quite as well optimized as traditional planar growth (e.g. thin-film growth). In addition to the challenge of obtaining well-defined QDs with certain size and abrupt interfaces, avoiding imperfections in the growth of the nanowire itself, such as changes in crystal structure or orientation [149, 179, 180], is also not trivial. Defects in crystal structure can create charge traps, affecting the local electrostatic environment of the QD and adversely affecting the single-photon emission properties [44]. In addition to states related to crystal structure defects, states related to the nanowire surface may also act as charge traps [181]. Therefore, surface passivation techniques (e.g. additional shell growth [182, 183] or ALD coating [184]), which prevent the formation of surface states within the bandgap range, could also be employed. Regardless of the difficulties in growth optimization, high-quality nanowires with QDs have been demonstrated with various material systems and techniques [156, 162, 171, 185].

One example of the state-of-the-art nanowire nanoantenna SPS fabrication can be found in Ref. [44]. The fabrication process can be roughly divided into the following steps: (i) deposition of SiO_2 growth mask layer on an InP substrate and patterning of openings filled with Au droplets (presumably by electron beam lithography, wet etching, Au evaporation, and lift-off as in Ref. [171]); (ii) InP nanowire axial growth with the InAsP QD insertion, and (iii) mixed InP axial and radial growth to cap the nanowire to the correct diameter for waveguiding and to obtain a tapered tip for efficient light extraction. Fabrication of the bottom mirror was omitted in this case but could be achieved by peeling off the nanowires in a polydimethylsiloxane (PDMS) film and depositing the mirror on the bottom side [186], or possibly by using an embedded Au mirror under the SiO_2 mask as proposed in

Ref. [116]. It is of note that the fabrication process here is considerably simpler than that for the micropillar cavity discussed in Section 5.1. On the other hand, this nanowire design does not include the possibility for emission tuning with an electric field.

It can further be noted here that, due to the high spatial symmetry, group III–V QDs in the [111] nanowire growth direction should exhibit vanishing FSS [65] and, therefore, also perform well as sources of entangled photon pairs via the biexciton–exciton radiative cascade. However, a nonvanishing FSS has actually been seen in experiments [187], which was attributed to compositional inhomogeneity in the ternary InAsP QD. Regardless, entangled photon pair emission has been demonstrated from InAsP QDs in bottom-up-grown InP nanowires in several papers [187–189]. The nanoantenna design is highly suitable for entangled photon pair sources as well, because of the relatively broadband effect of emission funneling into the guided mode [188].

6 State of the art

Nanowire SPSs following the nanoantenna design were experimentally demonstrated in 2010, first with top-down fabrication methods [113] and later with bottom-up growth [173], after which the approach has become quite ubiquitous for experimental bottom-up nanowire sources (see, e.g. Refs [44, 154, 171, 172, 186, 190, 191]). Experimental state-of-the-art results are discussed in the following, and Table 1 provides an overview of the obtained performance values. State-of-the-art results with top-down QD SPSs are also given for comparison. Brightness values are not included here because of the lack of comparable measurement conditions.

6.1 Single-photon purity

The highest reported single-photon purities in nanowire SPSs are getting close to the ideal $g^{(2)}(0) = 0$ value. For example, in Refs [171] and [44], optimized InP nanowire growth process resulted in strongly reduced stacking fault density (i.e. reduced charge trap density) in the vicinity of the InAsP QD. The reduced defect density resulted in reduced background emission and reduced spectral diffusion, providing improved single-photon purity of $g^{(2)}(0) < 0.01$ and narrower emission linewidth. In Ref. [171], some of the nonzero $g^{(2)}(0)$ was attributed to emission from other nanowires (spatial separation not large enough), while in Ref. [44] the re-excitation probability due to nonresonant excitation was considered to be the main limiting factor.

With top-down-fabricated designs, the best reported purities are even closer to the ideal case [47, 52, 92]. To the best of our knowledge, the highest ever single-photon purity was reported in Ref. [52], where raw (uncorrected) $g^{(2)}(0) = 0.000075(16)$ was obtained. The high purity was achieved with Al-droplet-etched GaAs QDs in a planar cavity structure by using resonant two-photon excitation of the biexciton state. The resonant two-photon excitation strongly suppresses QD re-excitation by a single pulse, and this was considered as the main factor in reaching the

Table 1: Current state-of-the-art SPSs with QDs embedded in bottom-up-grown nanowires and top-down-fabricated structures.

Reference	QD material system	Operation temperature	Excitation	Purity ($g^{(2)}(0)$)	Indistinguishability	Efficiency
Bottom-up-grown nanowire SPSs						
[44]	InAsP	300 mK	Nonresonant	<0.01[a]	0.83(2)[a,b]	0.43(4)
[31]	GaN	300 K	Nonresonant	0.33, 0.13[a]	–	–
[192]	GaN	350 K	Nonresonant	0.34(14), 0.06[a]	–	–
[177]	InGaN	25 K	Electrical	0.16[a]	–	–
Top-down-fabricated SPSs						
[47]	InGaAs	4 K	Resonant	0.0028(12)	0.989(4), 0.9956(45)[a]	0.16(2)[c]
[92]	InAs	7.8 K	Resonant	0.009(1)	0.964(3), 0.985(4)[a]	–
[102]	InGaAs	<15 K	Resonant	0.0092(4)[a]	0.73(1)[a,b]	0.74(4), 0.37(2)[c]
[52]	GaAs	4 K	Resonant	0.000075(16)	–	–
[100]	InAs	5 K	Nonresonant	0.31, 0.25[a]	–	0.75(1)
[72]	InGaN	280 K	Electrical	0.29[a]	–	0.02

This table gives the values as reported in the references including uncertainties if given. See Section 2 for the used performance metrics definitions.

[a]Corrected value. [b]Interference visibility reported instead of indistinguishability. [c]Linearly polarized.

high purity. Additionally, measuring such a low uncorrected $g^{(2)}(0)$ value required (i) the use of superconducting single-photon detectors with extremely low dark count rate and (ii) suppression of scattered excitation laser light by both notch filters and filtering by polarization direction. Note that all the high purity results mentioned here were obtained while using resonant excitation schemes, unlike in the nanowire examples.

6.2 Indistinguishability

High indistinguishability has been reported for bottom-up-grown sources employing InP nanowires with InAsP QDs [44, 193]. In Ref. [193], two-photon interference visibility of 0.787 was obtained with nonresonant excitation at 300 mK. Furthermore, in Ref. [44], excitation above the InP bandgap with high intensity was employed to fill the charge traps, leading to smaller fluctuation in the electrostatic environment of the QD and thus improving temporal coherence of the emission. This allowed the simultaneous demonstration of operation at the highest brightness and two-photon interference visibility of 0.83, although at 300 mK temperature and under temporal postselection (i.e. reduced time window). Interestingly, obtaining enhanced coherence at high pump laser intensity is opposite to the normally observed power broadening (e.g. in Refs [84, 194]). It was further proposed that the interference visibility could still be improved by using resonant excitation together with a separate laser or some other means for the charge-trap filling.

On the other hand, self-assembled QDs embedded in planar [58, 195, 196] or micropillar [47, 92, 102, 197] cavities have shown superior indistinguishability in excess of 0.9 and up to 0.9956 [47]. In addition to the effect of the cavity, indistinguishability was enhanced by resonant excitation schemes, namely resonant s-shell excitation [47, 58, 92, 102, 197], two-photon resonant excitation [195], and resonant excitation using adiabatic rapid passage with frequency-chirped pulses [196]. Moreover, micropillar cavity sources have demonstrated high indistinguishability over longer time scales [197, 198]. In Ref. [197], the indistinguishability remained above 0.88 for 39 consecutively emitted photons in 463 ns under resonant excitation and up to 0.7 for 33 consecutively emitted photons in 400 ns under nonresonant excitation. In Ref. [198], indistinguishability of 0.959(2) was obtained under resonant excitation with pulse separation of 13 ns, and it only decreased to 0.921(5) when increasing the pulse separation to 14.7 μs.

6.3 Efficiency

With the nanowire nanoantenna design, simultaneous optimization of all the factors at play in Eq. (5) is needed in order to achieve high extraction efficiency, which is not trivial in practice. Consequently, extraction efficiencies have not, to the best of our knowledge, reached the theoretical >90% values. For example, extraction efficiency of 42% was reported in Ref. [186], where the main limiting factor was considered to be the poor modal reflectivity of the bottom metallic mirror (around 30%). However, a top-down-fabricated nanowire nanoantenna reported in Ref. [113] reached 72% extraction efficiency. In this case, the bottom mirror contained a thin dielectric between the metal and the nanowire, which theoretically should yield modal reflectivity above 91%, while the main limiting factor was considered to be nonoptimal tapering in the tip. In Ref. [44], a bottom-up-grown nanowire nanoantenna with a fine taper toward the tip (tapering angle approximately 1°) yielded an overall efficiency of 43% without a bottom mirror. On the other hand, it has been successfully demonstrated that the nanoantenna design can be used to obtain Gaussian far-field emission pattern and high coupling efficiency to an optical fiber (i.e. after photon extraction from the nanowire), as reported in Ref. [190], where coupling efficiency of 93% was obtained.

The highest reported extraction efficiencies of top-down-fabricated SPSs are comparable to or even higher than those achieved so far with the nanoantenna. For example, with micropillar cavity designs, extraction efficiency of 65% was reported in Ref. [47], while in Ref. [102] a high overall efficiency of 74% together with 88% interference visibility was obtained. The simultaneous high efficiency and interference visibility were achieved via accurate alignment between the QD and micropillar and resonant excitation. Furthermore, adding stronger optical confinement for micropillars in the radial direction (e.g. by radial DBR stacks) has been considered to further suppress emission leaking to transverse radiation and thus increase the β-factor and extraction efficiency closer to 100% [199]. Coupling to optical fibers with high efficiency is also feasible. In Ref. [99], a photonic crystal waveguide design with a tapered outcoupler was used to achieve chip-to-fiber coupling efficiency exceeding 80%, while inverse conically tapered structures, the so-called photonic trumpets, were presented in Ref. [100] as another nanoantenna design (so far only realized by top-down fabrication) capable of Gaussian far-field emission. A proof-of-principle demonstration of a monolithic optical-fiber-coupled SPS has also been made, where such a photonic trumpet was detached from the substrate

and directly connected to the core of a fiber pigtail (the demonstrated efficiency at the output of the fiber pigtail was 5.8%) [200].

6.4 Room-temperature operation

So far, all of the discussed bottom-up nanowire SPSs have operated at cryogenic temperatures. However, efforts have been made to fabricate sources that would operate at room temperature. For this purpose, wide-bandgap materials have been employed, as these have sufficient band offsets and quantum confinement for excitons in the QD even at noncryogenic temperatures [31]. Some early demonstrations used II–VI materials such as CdSe QDs in ZnSe [71, 201], after which III–nitride materials have received more attention [31, 177, 202, 203]. However, the nanowire nanoantenna scheme has not been employed here, although axial QDs were used in Refs [202] and [177].

InGaN QDs were used in both Refs [202] and [177]. In Ref. [202], $In_{0.2}Ga_{0.8}N$ QDs in randomly nucleated $Al_{0.1}Ga_{0.9}N$ nanowires showed single-photon emission up to 200 K. In Ref. [177], $In_{0.25}Ga_{0.75}N$ QDs in randomly nucleated GaN nanowires showed electrically pumped, linearly polarized (degree of linear polarization = 70%) single-photon emission with $g^{(2)}(0) = 0.25$ at an estimated device temperature of 25 K. The GaN nanowires were doped to obtain a p–n diode, and single nanowires were detached from the growth substrate and transferred to an oxide-coated silicon wafer. The laterally lying nanowires were then electrically contacted for electrical pumping of single-photon emission.

In Ref. [31], GaN QDs inside GaN/AlGaN core–shell nanowires exhibited almost temperature-insensitive, optically pumped single-photon emission with $g^{(2)}(0) \approx 0.13$ up to 300 K. The nonzero $g^{(2)}(0)$ was mainly attributed to re-excitation of the QD within a single cycle because of the use of nonresonant excitation. The nanowires were fabricated on sapphire/AlN substrates via SAE in a MOVPE reactor such that the growth started with GaN core growth, followed by $Al_{0.8}Ga_{0.2}N$ shell growth, then a short GaN growth to form the QD and, finally, capping with $Al_xGa_{1-x}N$. The resulting structure then had the QD near the tip of the nanowire. The small size of the QD (height around 1 nm and width around 10 nm) also increased carrier confinement and exciton binding energy, and reduced the radiative lifetime. It was later demonstrated with similar nanowires that SPS operation was also possible at an elevated temperature of 350 K [192] and that the single-photon emission could be completely linearly polarized to within the experimental error [203]. Furthermore, it was noted that operation possibly up to gigahertz frequencies (due to the relatively short radiative lifetime), linear polarization, and high-temperature operation could make this system appealing for quantum information processing and quantum key distribution applications [31, 192, 203].

III–nitride materials have also been used in top-down SPSs. For example, in Ref. [72] an electrically pumped SPS diode structure was fabricated with an embedded self-assembled $In_{0.4}Ga_{0.6}N$ QD and exhibited emission in the red/visible wavelength range (around 630 nm) up to room temperature with $g^{(2)}(0) \approx 0.29$ (after corrections). The low single-photon purity was mainly attributed to spectral contamination from other states due to thermal broadening. On the other hand, even at 15 K, only $g^{(2)}(0) \approx 0.11$ was achieved. Moreover, the overall source efficiency was estimated to be only around 2%. Significantly improved single-photon purity (raw $g^{(2)}(0) = 0.085$) was recently obtained in Ref. [43] with interface fluctuation GaN QDs emitting at around 339 nm wavelength, but room-temperature operation was not yet demonstrated and no photonic structures were fabricated to improve emission and extraction efficiency. Some cavity structures have also been realized with III–nitride material systems. For example, in Ref. [204] InGaN QDs were grown via modified droplet epitaxy in MOVPE on an AlN/GaN DBR stack and capped with a SiO_x/SiN_x DBR stack to form a planar microcavity. However, single-photon emission was obtained around 433 nm with only $g^{(2)}(0) \approx 0.23$ at 4.2 K.

7 Current challenges and outlook

It is apparent from the state-of-the-art comparison that bottom-up nanowire sources tend to be outmatched, performance wise, by the other QD-based designs. Especially, micropillar cavity sources have exhibited simultaneously high purities and indistinguishabilities with moderately high extraction efficiencies [47, 92, 102]. Furthermore, a top-down-fabricated cavity-based source with electrical operation and 1550 nm telecom emission has been demonstrated [205]. Other designs with electric contacts allow for tuning of the emission by an applied electric field [47, 91, 206], even combined with integrated lasers for on-chip excitation [207]. However, the bottom-up nanowire sources offer, in principle, more straightforward, deterministic fabrication and more freedom with the material choices and compositions. It could be argued that, taking these fabrication benefits into account, bottom-up nanowire

SPSs are already a superior option for applications that require just efficient and pure single-photon generation regardless of indistinguishability.

Since the designs employing planar growth and top-down fabrication currently tend to have the edge in demonstrating both individually and simultaneously high values of purity and indistinguishability, one of the challenges for bottom-up nanowire sources is to improve their performance in order to provide a truly viable alternative. First, the fabrication and growth processes should be developed to simultaneously obtain optimized bottom mirrors and nanowires of high structural quality with optimized tapered tips in order to realize the theoretical extraction efficiencies exceeding 90%. Second, higher indistinguishability is needed. Unfortunately, in the presented nanoantenna scheme, it is not possible to obtain cavity structures with DBRs like in planar or top-down-etched micropillar designs. This is because the nanowire core diameter needs to be initially small to define the QD, and DBR stacks only in such a small diameter nanowire core are insufficient [114] (and forming a DBR stack in the axial direction during the radial growth is not feasible). Nanowire SPSs might still benefit from techniques already adopted elsewhere to improve performance. Especially, employing resonant s-shell excitation or the resonant two-photon excitation technique could considerably improve the purity and indistinguishability as seen in top-down fabricated SPSs. Some other techniques to investigate might include temporal filtering with amplitude modulation [94] and resonant excitation using adiabatic rapid passage with frequency-chirped pulses [196]. Additionally, QD emitter coupling to mechanical modes of the nanowire SPS structure might be worth investigating. Furthermore, the single nanowire nanoantenna design is not the only option. For example, in Ref. [208], a design with an annular-grating-patterned hyperbolic metamaterial in conjunction with nanowire QDs was proposed to provide both spontaneous emission enhancement and directional light output.

Another important area for improvement is the available emission wavelength range and tuning. For example, single-photon emission at the telecom 1550 nm wavelength using the InAsP material system is still challenging with bottom-up nanowires [172], whereas with top-down-fabricated SPSs emission at this wavelength was first demonstrated in 2005 [212]. The earlier demonstration with top-down-fabricated SPSs is largely due to the fact that planar growth and self-assembled Stranski–Krastanov QD growth processes are older and more well developed than nanowire QD growth. However, since the nanowire geometry allows much less stringent requirements for lattice matching, nanowire growth will have the edge in this regard if the growth processes can be optimized to a sufficiently high degree.

Perhaps a more important development direction then is to employ techniques for emission wavelength tuning, as it is still difficult to obtain several nanowires with QDs on the same chip with small enough inhomogeneous spectral broadening for applications requiring SPSs with certain wavelengths. QD emission tuning has been demonstrated in top-down designs with electric fields [47] and strain [213, 214]. Strain-tuning has been demonstrated with bottom-up nanowire SPSs as well [193]. Additionally, emission wavelength tuning with an external magnetic field [174] or by laser-induced material intermixing [215] has recently been reported for nanowire QDs. Although nanowire QD emission wavelength tuning with electric fields has been reported [216, 217], to the best of our knowledge, this has not been employed in nanowire SPSs.

Achieving electrical excitation with bottom-up nanowire nanoantenna SPSs also still remains a challenge. Since some of the potential applications would prefer electrical operation, this is an important problem to solve. Some designs for electrical operation have been proposed. For example, in Ref. [209], it was proposed that indium tin oxide (ITO) could be used as a transparent top contact, while ITO and gold could be used as both the bottom mirror and contact. A schematic illustration of this design is shown in Figure 5A. However, it is not trivial to combine an axial p–n or p–i–n junction with an embedded QD and the shell growth required for the proper diameter and the tapered tip.

Lastly, the integration of nanowire sources with other components is not straightforward. Since one of the most tangible benefits of the nanowire approach is the deterministic positioning of the QD, it would seem well suited for pursuing the realization of applications that require large-scale integration, such as integrated optical quantum information processing. Unfortunately, the vertical geometry of the nanowires, while naturally suited for vertical emission, is not a good match to the mostly planar components developed for integrated photonics.

One solution to this issue was proposed and demonstrated in Ref. [210], where nanowire nanoantenna sources were first fabricated on a separate substrate and then individually characterized, selected, and transferred to the device substrate with nanomanipulators. The nanowires could be laid on the substrate with defined locations and orientations, and the waveguides and other components could then be fabricated on top of the nanowires. The result of this scheme is illustrated in Figure 5B. While it was reported that the scheme worked well, one could argue that it is not very suitable for true large-scale

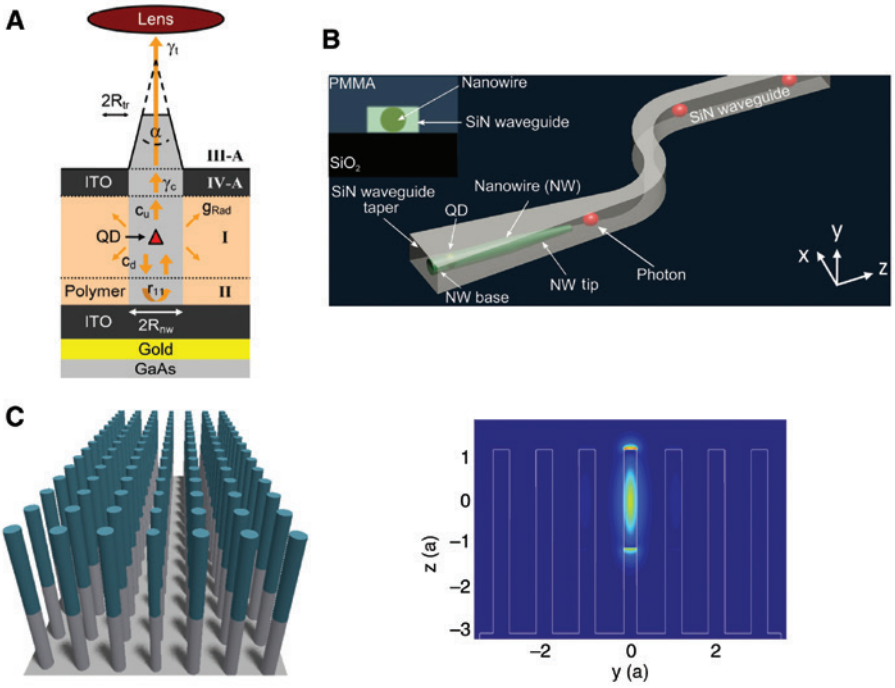

Figure 5: Illustrations of some proposed designs for future nanowire SPSs.
(A) Electrically operated nanowire SPS with ITO used as a transparent top contact. (B) Scheme for on-chip integration of a nanowire SPS with planar waveguide designs. Selected nanowire SPS is first transferred to the substrate with a nanomanipulator, after which the SiN waveguide is fabricated. (C) Photonic crystal waveguide structure (left) realized with nanowires (with the prospect of including one with an embedded QD) and simulated mode profile (right) showing additional vertical light confinement due to the nanowire heterostructure. Figure reprinted with permission from: (A) Ref. [209], 2010 by the Optical Society of America; (B) Ref. [210], 2016 by the American Chemical Society; (C) (left and right) Ref. [211], 2014 by the American Physical Society.

integration as the pick-and-place step with nanomanipulators is a delicate and slow serial process. A similar scheme was very recently reported [218], where the nanowire nanoantenna SPS was placed on top of a SiN waveguide such that on-chip optical pumping could couple from the waveguide to the nanowire and the SPS emission could couple from the nanowire to the waveguide. On the other hand, it would be possible to use nanowire sources in their natural vertical geometry if their emission could couple to a planar waveguide below or above the nanowires. There also exists a fabrication method for 3D waveguides in glass with femtosecond laser direct-writing [219], which could possibly be compatible with vertical nanowire sources. Furthermore, it is also possible to realize photonic crystal waveguides with nanowires [211], in which case both the waveguides and sources would be realized with nanowires. The nanowire photonic crystal waveguide and light confinement considered in Ref. [211] are illustrated in Figure 5C. Indeed, exploring novel schemes for integrating nanowires in their vertical geometry with other components, planar or otherwise, offers one interesting avenue for future research.

8 Conclusions

Bottom-up-grown nanowire SPSs benefit from deterministic positioning of both the embedded QD and the devices with respect to each other and have mostly followed the nanoantenna design, achieving rather impressive performance. Although it has not yet been experimentally demonstrated, the nanowire nanoantenna should be able to achieve extraction efficiency above 90%. It is also well suited for coupling the emission into an optical fiber because of the engineered Gaussian far-field emission pattern. Near-unity single-photon purity has been achieved, as well as relatively high indistinguishability and brightness. Furthermore, room-temperature operation has been achieved with III–nitride QDs.

However, despite this promising progress, presently the bottom-up-grown nanowire SPS approach has not demonstrated a clear advantage over top-down fabrication approaches. First, higher performance has been obtained with top-down designs, especially with regard to indistinguishability. Second, nanowires naturally assume a vertical shape and vertical emission direction, while most of the

components designed for integrated photonics are planar. Third, a single bottom-up-grown nanowire nanoantenna cannot presently incorporate a photonic cavity that arguably offers better ultimate indistinguishability–efficiency trade-off than a waveguide. However, the deterministic positioning is, at least currently, much more feasible in nanowires, and the nanowire growth process supports a wider variety of materials and compositions. It seems possible that both the bottom-up nanowire growth and top-down fabrication could be used in the future, with each approach being better suited for some specific applications.

Further research on nanowire-based SPSs is thus merited. In addition to improving the performance, tuning the emission wavelength with various strategies (e.g. strain and electric field) could be investigated further. For on-chip integrated applications, electrical excitation or on-chip optical excitation would be desirable, of which the former has not yet been achieved with the nanowire nanoantenna structure. Truly scalable fabrication process for integrated designs is also an important open issue that has not been tackled with top-down approaches either.

Acknowledgments: The authors acknowledge the financial support from Aalto ELEC doctoral school, Business Finland (FiDiPro: NP-Nano, OPEC, and A-Photonics), Academy of Finland (grants: 276376, 284548, 286920, 295777, 298297, 304666, 312297, 312551, 314810), Academy of Finland Flagship Programme (320167, PREIN), the European Union's Horizon 2020 research and innovation programme (820423, S2QUIP), and the Aalto Centre of Quantum Engineering. They thank the Micronova Nanofabrication Centre for providing the facilities.

References

[1] O'Brien JL, Furusawa A, Vučković J. Photonic quantum technologies. Nat Photonics 2009;3:687–95.
[2] Gisin N, Ribordy G, Tittel W, Zbinden H. Quantum cryptography. Rev Mod Phys 2002;74:145–95.
[3] Kimble HJ. The quantum internet. Nature 2008;453:1023–30.
[4] Northup TE, Blatt R. Quantum information transfer using photons. Nat Photonics 2014;8:356–63.
[5] Knill E, Laflamme R, Milburn GJ. A scheme for efficient quantum computation with linear optics. Nature 2001;409:46–52.
[6] Kok P, Munro WJ, Nemoto K, Ralph TC, Dowling JP, Milburn GJ. Linear optical quantum computing with photonic qubits. Rev Mod Phys 2007;79:135–74.
[7] Aspuru-Guzik A, Walther P. Photonic quantum simulators. Nat Phys 2012;8:285–91.
[8] Gol'Tsman GN, Okunev O, Chulkova G, et al. Picosecond superconducting single-photon optical detector. Appl Phys Lett 2001;79:705–7.
[9] Sprengers JP, Gaggero A, Sahin D, et al. Waveguide superconducting single-photon detectors for integrated quantum photonic circuits. Appl Phys Lett 2011;99:181110.
[10] Volz J, Scheucher M, Junge C, Rauschenbeutel A. Nonlinear π phase shift for single fibre-guided photons interacting with a single resonator-enhanced atom. Nat Photonics 2014;8:965–70.
[11] Rohde PP. Simple scheme for universal linear-optics quantum computing with constant experimental complexity using fiber loops. Phys Rev A 2015;91:012306.
[12] Takemoto K, Nambu Y, Miyazawa T, et al. Quantum key distribution over 120 km using ultrahigh purity single-photon source and superconducting single-photon detectors. Sci Rep 2015;5:14383.
[13] Bennett CH, Brassard G. Quantum cryptography: public key distribution and coin tossing. In: Proceedings of IEEE International Conference on Computers, Systems and Signal Processing. IEEE, Bangalore, India, 1984, pp. 175–9.
[14] Barbieri M, Weinhold TJ, Lanyon BP, et al. Parametric downconversion and optical quantum gates: two's company, four's a crowd. J. Mod Opt 2009;56:209–14.
[15] Takeoka M, Jin R-B, Sasaki M. Full analysis of multi-photon pair effects in spontaneous parametric down conversion based photonic quantum information processing. New J Phys 2015;17:043030.
[16] Aharonovich I, Englund D, Toth M. Solid-state single-photon emitters. Nat Photonics 2016;10:631–41.
[17] Kimble HJ, Dagenais M, Mandel L. Photon antibunching in resonance fluorescence. Phys Rev Lett 1977;39:691–5.
[18] Kuhn A, Hennrich M, Rempe G. Deterministic single-photon source for distributed quantum networking. Phys Rev Lett 2002;89:067901.
[19] Babinec TM, Hausmann BJM, Khan M. A diamond nanowire single-photon source. Nat Nanotechnol 2010;5:195–9.
[20] Marseglia L, Saha K, Ajoy A, et al. Bright nanowire single photon source based on SiV centers in diamond. Opt Express 2018;26:80–9.
[21] Tran TT, Elbadawi C, Totonjian D, et al. Robust multicolor single photon emission from point defects in hexagonal boron nitride. ACS Nano 2016;10:7331–8.
[22] Zhou Y, Wang Z, Rasmita A, et al. Room temperature solid-state quantum emitters in the telecom range. Sci Adv 2018;4:eaar3580.
[23] Buckley S, Rivoire K, Vučković J. Engineered quantum dot single-photon sources. Rep Prog Phys 2012;75:126503.
[24] Senellart P, Solomon G, White A. High-performance semiconductor quantum-dot single-photon sources. Nat Nanotechnol 2017;12:1026–39.
[25] Dietrich CP, Fiore A, Thompson MG, Kamp M, Höfling S. GaAs integrated quantum photonics: towards compact and multi-functional quantum photonic integrated circuits. Laser Photon Rev 2016;10:870–94.
[26] Bogdanov S, Shalaginov MY, Boltasseva A, Shalaev VM. Material platforms for integrated quantum photonics. Opt Mater Exp 2017;7:111–32.
[27] Dubrovskii VG. Understanding the vapor–liquid–solid growth and composition of ternary III–V nanowires and nanowire heterostructures. J Phys D Appl Phys 2017;50:453001.
[28] Royo M, De Luca M, Rurali R, Zardo I. A review on III–V core–multishell nanowires: growth, properties, and applications. J Phys D Appl Phys 2017;50:143001.

[29] Tomioka K, Ikejiri K, Tanaka T, et al. Selective-area growth of III–V nanowires and their applications. J Mater Res 2011;26:2127–41.
[30] Dalacu D, Mnaymneh K, Wu X, et al. Selective-area vapor–liquid–solid growth of tunable InAsP quantum dots in nanowires. Appl Phys Lett 2011;98:251101.
[31] Holmes MJ, Choi K, Kako S, Arita M, Arakawa Y. Room-temperature triggered single photon emission from a III-nitride site-controlled nanowire quantum dot. Nano Lett 2014;14:982–6.
[32] Maslov AV, Bakunov MI, Ning CZ. Distribution of optical emission between guided modes and free space in a semiconductor nanowire. J Appl Phys 2006;99:024314.
[33] Friedler I, Sauvan C, Hugonin JP, Lalanne P, Claudon J, Gérard JM. Solid-state single photon sources: the nanowire antenna. Opt Express 2009;17:2095–110.
[34] Lin X, Dai X, Pu C, et al. Electrically-driven single-photon sources based on colloidal quantum dots with near-optimal antibunching at room temperature. Nat Commun 2017;8:1132.
[35] Lodahl P, Mahmoodian S, Stobbe S. Interfacing single photons and single quantum dots with photonic nanostructures. Rev Mod Phys 2015;87:347–400.
[36] Gazzano O, Solomon GS. Toward optical quantum information processing with quantum dots coupled to microstructures. J Opt Soc Am B 2016;33:C160–75.
[37] Orieux A, Versteegh MAM, Jöns KD, Ducci S. Semiconductor devices for entangled photon pair generation: a review. Rep Prog Phys 2017;80:076001.
[38] Huber D, Reindl M, Aberl J, Rastelli A, Trotta R. Semiconductor quantum dots as an ideal source of polarization-entangled photon pairs on-demand: a review. J Opt 2018;20:073002.
[39] Stevens MJ. Photon statistics, measurements, and measurements tools. In: Single-Photon Generation and Detection: Physics and Applications. Ed. Migdall A, Polyakov S, Fan J, Bienfang JC. Experimental Methods in the Physical Sciences, Vol. 45. Academic Press, Elsevier Inc., 2013, Chapter 2, pp. 25–68.
[40] Hanbury Brown R, Twiss RQ. Correlation between photons in two coherent beams of light. Nature 1956;177:27–9.
[41] Muñoz-Matutano G, Barrera D, Fernández-Pousa CR, et al. All-optical fiber hanbury brown and twiss interferometer to study 1300 nm single photon emission of a metamorphic InAs quantum dot. Sci Rep 2016;6:27214.
[42] Brouri R, Beveratos A, Poizat J-P, Grangier P. Photon antibunching in the fluorescence of individual color centers in diamond. Opt Lett 2000;25:1294–6.
[43] Arita M, Le Roux F, Holmes MJ, Kako S, Arakawa Y. Ultraclean single photon emission from a GaN quantum dot. Nano Lett 2017;17:2902–7.
[44] Reimer ME, Bulgarini G, Fognini A, et al. Overcoming power broadening of the quantum dot emission in a pure wurtzite nanowire. Phys Rev B 2016;93:195316.
[45] Hong CK, Ou Z-Y, Mandel L. Measurement of subpicosecond time intervals between two photons by interference. Phys Rev Lett 1987;59:2044–6.
[46] Santori C, Fattal D, Vučković J, Solomon GS, Yamamoto Y. Indistinguishable photons from a single-photon device. Nature 2002;419:594–7.
[47] Somaschi N, Giesz V, De Santis L, et al. Near-optimal single-photon sources in the solid state. Nat Photonics 2016;10:340–5.
[48] Fearn H, Loudon R. Theory of two-photon interference. J Opt Soc Am B 1989;6:917–27.
[49] Patel RB, Bennett AJ, Cooper K, et al. Postselective two-photon interference from a continuous nonclassical stream of photons emitted by a quantum dot. Phys Rev Lett 2008;100:207405.
[50] Flagg EB, Polyakov SV, Thomay T, Solomon GS. Dynamics of nonclassical light from a single solid-state quantum emitter. Phys Rev Lett 2012;109:163601.
[51] Cao H, Ma J, Huang L. Design and synthesis of antiblinking and antibleaching quantum dots in multiple colors via wave function confinement. J Am Chem Soc 2016;138:15727–35.
[52] Schweickert L, Jöns KD, Zeuner KD, et al. On-demand generation of background-free single photons from a solid-state source. Appl Phys Lett 2018;112:093106.
[53] Hu YZ, Koch SW, Lindberg M, Peyghambarian N, Pollock EL, Abraham FF. Biexcitons in semiconductor quantum dots. Phys Rev Lett 1990;64:1805–7.
[54] Gérard J-M, Gayral B. Strong purcell effect for InAs quantum boxes in three-dimensional solid-state microcavities. J Lightwave Technol 1999;17:2089–95.
[55] Yuan X, Weyhausen-Brinkmann F, Martín-Sánchez J, et al. Uniaxial stress flips the natural quantization axis of a quantum dot for integrated quantum photonics. Nat Commun 2018;9:3058.
[56] Elshaari AW, Zadeh IE, Fognini A, et al. On-chip single photon filtering and multiplexing in hybrid quantum photonic circuits. Nat Commun 2017;8:379.
[57] Melet R, Voliotis V, Enderlin A, et al. Resonant excitonic emission of a single quantum dot in the Rabi regime. Phys Rev B 2008;78:073301.
[58] He Y-M, He Y, Wei Y-J, et al. On-demand semiconductor single-photon source with near-unity indistinguishability. Nat Nanotechnol 2013;8:213–7.
[59] Kalliakos S, Brody Y, Bennett AJ, et al. Enhanced indistinguishability of in-plane single photons by resonance fluorescence on an integrated quantum dot. Appl Phys Lett 2016;109:151112.
[60] Sapienza L, Davanço M, Badolato A, Srinivasan K. Nanoscale optical positioning of single quantum dots for bright and pure single-photon emission. Nat Commun 2015;6:7833.
[61] Hanschke L, Fischer KA, Appel S, et al. Quantum dot single-photon sources with ultra-low multi-photon probability. npj Quantum Inf 2018;4:43.
[62] Benson O, Santori C, Pelton M, Yamamoto Y. Regulated and entangled photons from a single quantum dot. Phys Rev Lett 2000;84:2513–6.
[63] Moreau E, Robert I, Manin L, Thierry-Mieg V, Gérard JM, Abram I. Quantum cascade of photons in semiconductor quantum dots. Phys Rev Lett 2001;87:183601.
[64] Gammon D, Snow ES, Shanabrook BV, Katzer DS, Park D. Fine structure splitting in the optical spectra of single GaAs quantum dots. Phys Rev Lett 1996;76:3005–8.
[65] Singh R, Bester G. Nanowire quantum dots as an ideal source of entangled photon pairs. Phys Rev Lett 2009;103:063601.
[66] Bennett AJ, Pooley MA, Stevenson RM, et al. Electric-field-induced coherent coupling of the exciton states in a single quantum dot. Nat Phys 2010;6:947–50.
[67] Winik R, Cogan D, Don Y, et al. On-demand source of maximally entangled photon pairs using the biexciton-exciton radiative cascade. Phys Rev B 2017;95:235435.
[68] Müller M, Bounouar S, Jöns KD, Glässl M, Michler P. On-demand generation of indistinguishable polarization-entangled photon pairs. Nat Photonics 2014;8:224–8.

[69] Besombes L, Kheng K, Marsal L, Mariette H. Acoustic phonon broadening mechanism in single quantum dot emission. Phys Rev B 2001;63:155307.
[70] Favero I, Cassabois G, Ferreira R, et al. Acoustic phonon sidebands in the emission line of single InAs/GaAs quantum dots. Phys Rev B 2003;68:233301.
[71] Bounouar S, Elouneg-Jamroz M, den Hertog M, et al. Ultrafast room temperature single-photon source from nanowire-quantum dots. Nano Lett 2012;12:2977–81.
[72] Deshpande S, Frost T, Hazari A, Bhattacharyaa P. Electrically pumped single-photon emission at room temperature from a single InGaN/GaN quantum dot. Appl Phys Lett 2014;105:141109.
[73] Grange T. Decoherence in quantum dots due to real and virtual transitions: a nonperturbative calculation. Phys Rev B 2009;80:245310.
[74] Thoma A, Schnauber P, Gschrey M, et al. Exploring dephasing of a solid-state quantum emitter via time- and temperature-dependent Hong-Ou-Mandel experiments. Phys Rev Lett 2016;116:033601.
[75] Grange T, Somaschi N, Antón C, et al. Reducing phonon-induced decoherence in solid-state single-photon sources with cavity quantum electrodynamics. Phys Rev Lett 2017;118:253602.
[76] Iles-Smith J, McCutcheon DPS, Nazir A, Mørk J. Phonon scattering inhibits simultaneous near-unity efficiency and indistinguishability in semiconductor single-photon sources. Nat Photonics 2017;11:521–6.
[77] Kuhlmann AV, Houel J, Ludwig A, et al. Charge noise and spin noise in a semiconductor quantum device. Nat Phys 2013;9:570–5.
[78] Kuhlmann AV, Prechtel JH, Houel J, et al. Transform-limited single photons from a single quantum dot. Nat Commun 2015;6:8204.
[79] Berthelot A, Favero I, Cassabois G, et al. Unconventional motional narrowing in the optical spectrum of a semiconductor quantum dot. Nat Phys 2006;2:759–64.
[80] Favero I, Berthelot A, Cassabois G, et al. Temperature dependence of the zero-phonon linewidth in quantum dots: an effect of the fluctuating environment. Phys Rev B 2007;75:073308.
[81] Sallen G, Tribu A, Aichele T, et al. Subnanosecond spectral diffusion of a single quantum dot in a nanowire. Phys Rev B 2011;84:041405.
[82] Bounouar S, Trichet A, Elouneg-Jamroz M, et al. Extraction of the homogeneous linewidth of the spectrally diffusing line of a CdSe/ZnSe quantum dot embedded in a nanowire. Phys Rev B 2012;86:085325.
[83] Munsch M, Kuhlmann AV, Cadeddu D, et al. Resonant driving of a single photon emitter embedded in a mechanical oscillator. Nat Commun 2017;8:76.
[84] Gazzano O, Michaelis de Vasconcellos S, Arnold C, et al. Bright solid-state sources of indistinguishable single photons. Nat Commun 2013;4:1425.
[85] Varoutsis S, Laurent S, Kramper P, et al. Restoration of photon indistinguishability in the emission of a semiconductor quantum dot. Phys Rev B 2005;72:041303(R).
[86] Barnes WL, Björk G, Gérard JM, et al. Solid-state single photon sources: light collection strategies. Eur Phys J D – Atom Mol Opt Plasma Phys 2002;18:197–210.
[87] Gérard JM, Sermage B, Gayral B, Legrand B, Costard E, Thierry-Mieg V. Enhanced spontaneous emission by quantum boxes in a monolithic optical microcavity. Phys Rev Lett 1998;81:1110–3.
[88] Moreau E, Robert I, Gérard JM, Abram I, Manin L, Thierry-Mieg V. Single-mode solid-state single photon source based on isolated quantum dots in pillar microcavities. Appl Phys Lett 2001;79:2865–7.
[89] Pelton M, Santori C, Vucković J, et al. Efficient source of single photons: a single quantum dot in a micropost microcavity. Phys Rev Lett 2002;89:233602.
[90] Böckler C, Reitzenstein S, Kistner C, et al. Electrically driven high-Q quantum dot-micropillar cavities. Appl Phys Lett 2008;92:091107.
[91] Nowak AK, Portalupi SL, Giesz V, et al. Deterministic and electrically tunable bright single-photon source. Nat Commun 2014;5:3240.
[92] Ding X, He Y, Duan Z-C, et al. On-demand single photons with high extraction efficiency and near-unity indistinguishability from a resonantly driven quantum dot in a micropillar. Phys Rev Lett 2016;116:020401.
[93] Michler P, Kiraz A, Becher C, et al. A quantum dot single-photon turnstile device. Science 2000;290:2282–5.
[94] Ates S, Agha I, Gulinatti A, Rech I, Badolato A, Srinivasan K. Improving the performance of bright quantum dot single photon sources using temporal filtering via amplitude modulation. Sci Rep 2013;3:1397.
[95] Laurent S, Varoutsis S, Le Gratiet L, et al. Indistinguishable single photons from a single-quantum dot in a two-dimensional photonic crystal cavity. Appl Phys Lett 2005;87:163107.
[96] Luxmoore IJ, Toro R, Del Pozo-Zamudio O, et al. III–V quantum light source and cavity-QED on Silicon. Sci Rep 2013;3:1239.
[97] Madsen KH, Ates S, Liu J, et al. Efficient out-coupling of high-purity single photons from a coherent quantum dot in a photonic-crystal cavity. Phys Rev B 2014;90:155303.
[98] Arcari M, Söllner I, Javadi A, et al. Near-unity coupling efficiency of a quantum emitter to a photonic crystal waveguide. Phys Rev Lett 2014;113:093603.
[99] Daveau RS, Balram KC, Pregnolato T, et al. Efficient fiber-coupled single-photon source based on quantum dots in a photonic-crystal waveguide. Optica 2017;4:178–84.
[100] Munsch M, Malik NS, Dupuy E, et al. Dielectric GaAs antenna ensuring an efficient broadband coupling between an InAs quantum dot and a Gaussian optical beam. Phys Rev Lett 2013;110:177402.
[101] Takemoto K, Takatsu M, Hirose S, et al. An optical horn structure for single-photon source using quantum dots at telecommunication wavelength. J Appl Phys 2007;101:081720.
[102] Unsleber S, He Y-M, Gerhardt S, et al. Highly indistinguishable on-demand resonance fluorescence photons from a deterministic quantum dot micropillar device with 74% extraction efficiency. Opt Express 2016;24:8539–46.
[103] Purcell EM. Spontaneous emission probabilities at radio frequencies. Phys Rev 1946;69:681.
[104] Bleuse J, Claudon J, Creasey M, et al. Inhibition, enhancement, and control of spontaneous emission in photonic nanowires. Phys Rev Lett 2011;106:103601.
[105] Reithmaier JP, Sek G, Löffler A, et al. Strong coupling in a single quantum dot–semiconductor microcavity system. Nature 2004;432:197–200.

[106] Laucht A, Hofbauer F, Hauke N, et al. Electrical control of spontaneous emission and strong coupling for a single quantum dot. New J Phys 2009;11:023034.
[107] Bennett AJ, Patel RB, Skiba-Szymanska J, et al. Giant Stark effect in the emission of single semiconductor quantum dots. Appl Phys Lett 2010;97:031104.
[108] Alén B, Bosch J, Granados D, Martínez-Pastor J, García JM, González L. Oscillator strength reduction induced by external electric fields in self-assembled quantum dots and rings. Phys Rev B 2007;75:045319.
[109] Söllner I, Mahmoodian S, Hansen SL, et al. Deterministic photon–emitter coupling in chiral photonic circuits. Nat Nanotechnol 2015;10:775–8.
[110] Gudiksen MS, Lauhon LJ, Wang J, Smith DC, Lieber CM. Growth of nanowire superlattice structures for nanoscale photonics and electronics. Nature 2002;415:617–20.
[111] Borgström MT, Zwiller V, Müller E, Imamoglu A. Optically bright quantum dots in single nanowires. Nano Lett 2005;5:1439–43.
[112] Dorenbos SN, Sasakura H, Van Kouwen MP, et al. Position controlled nanowires for infrared single photon emission. Appl Phys Lett 2010;97:171106.
[113] Claudon J, Bleuse J, Malik NS, et al. A highly efficient single-photon source based on a quantum dot in a photonic nanowire. Nat Photonics 2010;4:174–7.
[114] Friedler I, Lalanne P, Hugonin JP, et al. Efficient photonic mirrors for semiconductor nanowires. Opt Lett 2008;33:2635–7.
[115] Gregersen N, Nielsen TR, Claudon J, Gérard J-M, Mørk J. Controlling the emission profile of a nanowire with a conical taper. Opt Lett 2008;33:1693–5.
[116] Claudon J, Gregersen N, Lalanne P, Gérard JM. Harnessing light with photonic nanowires: fundamentals and applications to quantum optics. Chem Phys Chem 2013;14:2393–402.
[117] Mårtensson T, Borgström M, Seifert W, Ohlsson BJ, Samuelson L. Fabrication of individually seeded nanowire arrays by vapour–liquid–solid growth. Nanotechnology 2003;14:1255–8.
[118] Mårtensson T, Carlberg P, Borgström M, Montelius L, Seifert W, Samuelson L. Nanowire arrays defined by nanoimprint lithography. Nano Lett 2004;4:699–702.
[119] Rivera T, Debray JP, Gérard JM, Legrand B, Manin-Ferlazzo L, Oudar JL. Optical losses in plasma-etched AlGaAs microresonators using reflection spectroscopy. Appl Phys Lett 1999;74:911–3.
[120] Goldstein L, Glas F, Marzin JY, Charasse MN, Le Roux G. Growth by molecular beam epitaxy and characterization of InAs/GaAs strained-layer superlattices. Appl Phys Lett 1985;47:1099–101.
[121] Alloing B, Zinoni C, Li LH, Fiore A, Patriarche G. Structural and optical properties of low-density and In-rich InAs/GaAs quantum dots. J Appl Phys 2007;101:024918.
[122] Löffler A, Reithmaier J-P, Forchel A, et al. Influence of the strain on the formation of GaInAs/GaAs quantum structures. J Cryst Growth 2006;286:6–10.
[123] Garcıa JM, Mankad T, Holtz PO, Wellman PJ, Petroff PM. Electronic states tuning of InAs self-assembled quantum dots. Appl Phys Lett 1998;72:3172–4.
[124] Olbrich F, Höschele J, Müller M, et al. Polarization-entangled photons from an InGaAs-based quantum dot emitting in the telecom C-band. Appl Phys Lett 2017;111:133106.
[125] Thon SM, Rakher MT, Kim H, et al. Strong coupling through optical positioning of a quantum dot in a photonic crystal cavity. Appl Phys Lett 2009;94:111115.
[126] Dousse A, Lanco L, Suffczynski J, et al. Controlled light-matter coupling for a single quantum dot embedded in a pillar microcavity using far-field optical lithography. Phys Rev Lett 2008;101:267404.
[127] Kiravittaya S, Rastelli A, Schmidt OG. Advanced quantum dot configurations. Rep Prog Phys 2009;72:046502.
[128] Huggenberger A, Schneider C, Drescher C, et al. Site-controlled In(Ga)As/GaAs quantum dots for integration into optically and electrically operated devices. J Cryst Growth 2011;323:194–7.
[129] Tommila J, Strelow C, Schramm A, et al. The influence of temperature on the photoluminescence properties of single InAs quantum dots grown on patterned GaAs. Nanoscale Res Lett 2012;7:313.
[130] Schneider C, Huggenberger A, Sünner T, et al. Single site-controlled In(Ga)As/GaAs quantum dots: growth, properties and device integration. Nanotechnology 2009;20:434012.
[131] Jöns KD, Atkinson P, Müller M, et al. Triggered indistinguishable single photons with narrow line widths from site-controlled quantum dots. Nano Lett 2013;13:126–30.
[132] Canet-Ferrer J, Munoz-Matutano G, Herranz J, et al. Exciton and multiexciton optical properties of single InAs/GaAs site-controlled quantum dots. Appl Phys Lett 2013;103:183112.
[133] Dalacu D, Reimer ME, Fréderick S, et al. Directed self-assembly of single quantum dots for telecommunication wavelength optical devices. Laser Photon Rev 2010;4:283–99.
[134] Juska G, Dimastrodonato V, Mereni LO, Gocalinska A, Pelucchi E. Towards quantum-dot arrays of entangled photon emitters. Nat Photonics 2013;7:527–31.
[135] Kästner G, Gösele U. Stress and dislocations at cross-sectional heterojunctions in a cylindrical nanowire. Philos Mag 2004;84:3803–24.
[136] Chuang LC, Moewe M, Chase C, Kobayashi NP, Chang-Hasnain C, Crankshaw S. Critical diameter for III–V nanowires grown on lattice-mismatched substrates. Appl Phys Lett 2007;90:043115.
[137] Glas F. Critical dimensions for the plastic relaxation of strained axial heterostructures in free-standing nanowires. Phys Rev B 2006;74:121302(R).
[138] Fortuna SA, Li X. Metal-catalyzed semiconductor nanowires: a review on the control of growth directions. Semicond Sci Technol 2010;25:024005.
[139] Joyce HJ, Wong-Leung J, Gao Q, Hoe Tan H, Jagadish C. Phase perfection in zinc blende and wurtzite III–V nanowires using basic growth parameters. Nano Lett 2010;10:908–15.
[140] Fontcuberta i Morral A. Gold-free GaAs nanowire synthesis and optical properties. IEEE J Sel Top Quantum Electron 2011;17:819–28.
[141] Dick KA. A review of nanowire growth promoted by alloys and non-alloying elements with emphasis on Au-assisted III–V nanowires. Prog Cryst Growth Charact Mater 2008;54:138–73.
[142] Bauer B, Rudolph A, Soda M, et al. Position controlled self-catalyzed growth of GaAs nanowires by molecular beam epitaxy. Nanotechnology 2010;21:435601.
[143] Wagner RS, Ellis WC. Vapor–liquid–solid mechanism of single crystal growth. Appl Phys Lett 1964;4:89–90.

[144] Givargizov EI. Fundamental aspects of VLS growth. In: Vapour Growth and Epitaxy. Ed. Cullen GW, Kaldis E, Parker RL, Rooymans CJM. Elsevier, Amsterdam, 1975, pp. 20–30. isbn: 978-1-4831-9854-5. doi: 10.1016/B978-1-4831-9854-5.50006–9.
[145] Hiruma K, Katsuyama T, Ogawa K, Koguchi M, Kakibayashi H, Morgan GP. Quantum size microcrystals grown using organometallic vapor phase epitaxy. Appl Phys Lett 1991;59:431–3.
[146] Yazawa M, Koguchi M, Muto A, Ozawa M, Hiruma K. Effect of one monolayer of surface gold atoms on the epitaxial growth of InAs nanowhiskers. Appl Phys Lett 1992;61:2051–3.
[147] Seifert W, Borgström M, Deppert K, et al. Growth of one-dimensional nanostructures in MOVPE. J Cryst Growth 2004;272:211–20.
[148] Dick KA, Deppert K, Karlsson LS, Wallenberg LR, Samuelson L, Seifert W. A new understanding of Au-assisted growth of III–V semiconductor nanowires. Adv Funct Mater 2005;15:1603–10.
[149] Dick KA, Caroff P, Bolinsson J, et al. Control of III–V nanowire crystal structure by growth parameter tuning. Semicond Sci Technol 2010;25:024009.
[150] Krogstrup P, Jørgensen HI, Johnson E, et al. Advances in the theory of III–V nanowire growth dynamics. J Phys D Appl Phys 2013;46:313001.
[151] Dubrovskii VG. Development of growth theory for vapor–liquid–solid nanowires: contact angle, truncated facets, and crystal phase. Cryst Growth Des 2017;17:2544–8.
[152] Glas F. Comparison of modeling strategies for the growth of heterostructures in III–V nanowires. Cryst Growth Des 2017;17:4785–94.
[153] Plante MC, LaPierre RR. Control of GaAs nanowire morphology and crystal structure. Nanotechnology 2008;19:495603.
[154] Bulgarini G, Reimer ME, Zehender T, et al. Spontaneous emission control of single quantum dots in bottom-up nanowire waveguides. Appl Phys Lett 2012;100:121106.
[155] Wallentin J, Borgström MT. Doping of semiconductor nanowires. J Mater Res 2011;26:2142–56.
[156] Tateno K, Zhang G, Gotoh H, Sogawa T. VLS growth of alternating InAsP/InP heterostructure nanowires for multiple-quantum-dot structures. Nano Lett 2012;12:2888–93.
[157] Ikejiri K, Noborisaka J, Hara S, Motohisa J, Fukui T. Mechanism of catalyst-free growth of GaAs nanowires by selective area MOVPE. J Cryst Growth 2007;298:616–9.
[158] Motohisa J, Noborisaka J, Takeda J, Inari M, Fukui T. Catalyst-free selective-area MOVPE of semiconductor nanowires on (111)B oriented substrates. J Cryst Growth 2004;272:180–5.
[159] Gao Q, Saxena D, Wang F, et al. Selective-area epitaxy of pure wurtzite InP nanowires: high quantum efficiency and room-temperature lasing. Nano Lett 2014;14:5206–11.
[160] Hertenberger S, Rudolph D, Bichler M, Finley JJ, Abstreiter G, Koblmüller G. Growth kinetics in position-controlled and catalyst-free InAs nanowire arrays on Si(111) grown by selective area molecular beam epitaxy. J Appl Phys 2010;108:114316.
[161] Kitauchi Y, Kobayashi Y, Tomioka K, et al. Structural transition in indium phosphide nanowires. Nano Lett 2010;10:1699–703.
[162] Tatebayashi J, Ota Y, Ishida S, Nishioka M, Iwamoto S, Arakawa Y. Highly uniform, multi-stacked InGaAs/GaAs quantum dots embedded in a GaAs nanowire. Appl Phys Lett 2014;105:103104.
[163] Bassett KP, Mohseni PK, Li X. Evolution of GaAs nanowire geometry in selective area epitaxy. Appl Phys Lett 2015;106:133102.
[164] Kohashi Y, Sakita S, Hara S, Motohisa J. Pitch-independent realization of 30-nm-diameter InGaAs nanowire arrays by two-step growth method in selective-area metalorganic vapor-phase epitaxy. Appl Phys Express 2013;6:025502.
[165] Kohashi Y, Sato T, Ikejiri K, Tomioka K, Hara S, Motohisa J. Influence of growth temperature on growth of InGaAs nanowires in selective-area metal–organic vapor-phase epitaxy. J Cryst Growth 2012;338:47–51.
[166] Jeannin M, Crémel T, Häyrynen T, et al. Enhanced photon extraction from a nanowire quantum dot using a bottom-up photonic shell. Phys Rev Appl 2017;8:054022.
[167] Fröberg LE, Wacaser BA, Wagner JB, et al. Transients in the formation of nanowire heterostructures. Nano Lett 2008;8:3815–8.
[168] Dick KA, Bolinsson J, Borg BM, Johansson J. Controlling the abruptness of axial heterojunctions in III–V nanowires: beyond the reservoir effect. Nano Lett 2012;12:3200–6.
[169] Dubrovskii VG, Sibirev NV. Factors influencing the interfacial abruptness in axial III–V nanowire heterostructures. Cryst Growth Des 2016;16:2019–23.
[170] Khoshnegar M, Huber T, Predojević A, et al. A solid state source of photon triplets based on quantum dot molecules. Nat Commun 2017;8:15716.
[171] Dalacu D, Mnaymneh K, Lapointe J, et al. Ultraclean emission from InAsP quantum dots in defect-free wurtzite InP nanowires. Nano Lett 2012;12:5919–23.
[172] Haffouz S, Zeuner KD, Dalacu D, et al. Bright single InAsP quantum dots at telecom wavelengths in position-controlled InP nanowires: the role of the photonic waveguide. Nano Lett 2018;18:3047–52.
[173] Heinrich J, Huggenberger A, Heindel T, et al. Single photon emission from positioned GaAs/AlGaAs photonic nanowires. Appl Phys Lett 2010;96:211117.
[174] Leandro L, Gunnarsson CP, Reznik R, et al. Nanowire quantum dots tuned to atomic resonances. Nano Lett 2018;18:7217–21.
[175] Lazić S, Chernysheva E, Gačević Ž, et al. Ordered arrays of InGaN/GaN dot-in-a-wire nanostructures as single photon emitters. In: Chyi J-I, Fujioka H, Morkoç H, eds. Gallium Nitride Materials and Devices X. Proceedings of SPIE, Vol. 9363. International Society for Optics and Photonics. SPIE, 2015, 93630U. doi: 10.1117/12.2074898.
[176] Plissard S, Larrieu G, Wallart X, Caroff P. High yield of self-catalyzed GaAs nanowire arrays grown on silicon via gallium droplet positioning. Nanotechnology 2011;22:275602.
[177] Deshpande S, Heo J, Das A, Bhattacharya P. Electrically driven polarized single-photon emission from an InGaN quantum dot in a GaN nanowire. Nature Commun 2013;4:1675.
[178] Kuyanov P, LaPierre RR. Photoluminescence and photocurrent from InP nanowires with InAsP quantum dots grown on Si by molecular beam epitaxy. Nanotechnology 2015;26:315202.
[179] Jacobsson D, Panciera F, Tersoff J, et al. Interface dynamics and crystal phase switching in GaAs nanowires. Nature 2016 531:317–22.
[180] Liu Z, Merckling C, Rooyackers R, et al. Correlation between surface reconstruction and polytypism in InAs nanowire selective area epitaxy. Phys Rev Mater 2017;1:074603.
[181] Demichel O, Heiss M, Bleuse J, Mariette H, Fontcuberta i Morral A. Impact of surfaces on the optical properties of GaAs nanowires. Appl Phys Lett 2010;97:201907.
[182] Chang C-C, Chi C-Y, Yao M, et al. Electrical and optical characterization of surface passivation in GaAs nanowires. Nano Lett 2012;12:4484–9.

[183] Haggren T, Jiang H, Kakko J-P, et al. Strong surface passivation of GaAs nanowires with ultrathin InP and GaP capping layers. Appl Phys Lett 2014;105:033114.
[184] Dhaka V, Perros A, Naureen S, et al. Protective capping and surface passivation of III–V nanowires by atomic layer deposition. AIP Adv 2016;6:015016.
[185] Priante G, Patriarche G, Oehler F, Glas F, Harmand J-C. Abrupt GaP/GaAs interfaces in self-catalyzed nanowires. Nano Lett 2015;15:6036–41.
[186] Reimer ME, Bulgarini G, Akopian N, et al. Bright single-photon sources in bottom-up tailored nanowires. Nat Commun 2012;3:737.
[187] Huber T, Predojević A, Khoshnegar M, et al. Polarization entangled photons from quantum dots embedded in nanowires. Nano Lett 2014;14:7107–14.
[188] Versteegh MAM, Reimer ME, Jöns KD, et al. Observation of strongly entangled photon pairs from a nanowire quantum dot. Nat Commun 2014;5:5298.
[189] Jöns KD, Schweickert L, Versteegh MAM, et al. Bright nanoscale source of deterministic entangled photon pairs violating Bell's inequality. Sci Rep 2017;7:1700.
[190] Bulgarini G, Reimer ME, Bavinck MB, et al. Nanowire waveguides launching single photons in a gaussian mode for ideal fiber coupling. Nano Lett 2014;14:4102–6.
[191] Yanase S, Sasakura H, Hara S, Motohisa J. Single-photon emission from InAsP quantum dots embedded in density-controlled InP nanowires. Jpn J Appl Phys 2017;56:04CP04.
[192] Holmes MJ, Kako S, Choi K, Arita M, Arakawa Y. Single photons from a hot solid-state emitter at 350 K. ACS Photon 2016;3:543–6.
[193] Chen Y, Zadeh IE, Jöns KD, et al. Controlling the exciton energy of a nanowire quantum dot by strain fields. Appl Phys Lett 2016;108:182103.
[194] Bennett AJ, Unitt DC, Shields AJ, Atkinson P, Ritchie DA. Influence of exciton dynamics on the interference of two photons from a microcavity single-photon source. Opt Express 2005;13:7772–8.
[195] Huber D, Reindl M, Huo Y, et al. Highly indistinguishable and strongly entangled photons from symmetric GaAs quantum dots. Nat Commun 2017;8:15506.
[196] Wei Y-J, He Y-M, Chen M-C, et al. Deterministic and robust generation of single photons from a single quantum dot with 99.5% indistinguishability using adiabatic rapid passage. Nano Lett 2014;14:6515–9.
[197] Loredo JC, Zakaria NA, Somaschi N, et al. Scalable performance in solid-state single-photon sources. Optica 2016;3:433–40.
[198] Wang H, Duan ZC, Li YH, et al. Near-transform-limited single photons from an efficient solid-state quantum emitter. Phys Rev Lett 2016;116:213601.
[199] Jakubczyk T, Franke H, Smoleński T, et al. Inhibition and enhancement of the spontaneous emission of quantum dots in micropillar cavities with radial-distributed Bragg reflectors. ACS Nano 2014;8:9970–8.
[200] Cadeddu D, Teissier J, Braakman FR, et al. A fiber-coupled quantum-dot on a photonic tip. Appl Phys Lett 2016;108:011112.
[201] Tribu A, Sallen G, Aichele T, et al. A high-temperature single-photon source from nanowire quantum dots. Nano Lett 2008;8:4326–9.
[202] Deshpande S, Das A, Bhattacharya P. Blue single photon emission up to 200 K from an InGaN quantum dot in AlGaN nanowire. Appl Phys Lett 2013;102:161114.
[203] Holmes MJ, Kako S, Choi K, Arita M, Arakawa Y. Linearly polarized single photons from small site-controlled GaN nanowire quantum dots. In: Chyi J-I, Fujioka H, Morkoç H, Nanishi Y, Schwarz UT, eds. Jong-In Shim Gallium Nitride Materials and Devices XI. Proceedings of SPIE, Vol. 9748. International Society for Optics and Photonics. SPIE, 2016, 97481E. doi: 10.1117/12.2212455.
[204] Oliver RA, Jarjour AF, Taylor RA, et al. Growth and assessment of InGaN quantum dots in a microcavity: a blue single photon source. Mater Sci Eng B 2008;147:108–13.
[205] Miyazawa T, Okumura S, Hirose S, et al. First demonstration of electrically driven 1.55 μm single-photon generator. Jpn J Appl Phys 2008;47:2880–3.
[206] Strauf S, Stoltz NG, Rakher MT, Coldren LA, Petroff PM, Bouwmeester D. High-frequency single-photon source with polarization control. Nat Photonics 2007;1:704–8.
[207] Munnelly P, Heindel T, Thoma A, et al. Electrically tunable single-photon source triggered by a monolithically integrated quantum dot microlaser. ACS Photon 2017;4:790–4.
[208] Chen F, Li Q, Li M, Zhang H, Huang F, Zhang J. Grating-patterned hyperbolic metamaterials for InGaN/GaN nanowire quantum dots single photon source. In: Piprek J, Willatzen M, eds. 2017 International Conference on Numerical Simulation of Optoelectronic Devices (NUSOD). IEEE, 2017, pp. 99–100. doi: 10.1109/NUSOD.2017.8010010.
[209] Gregersen N, Nielsen TR, Mørk J, Claudon J, Gérard J-M. Designs for high-efficiency electrically pumped photonic nanowire single-photon sources. Opt Express 2010;18:21204–18.
[210] Zadeh IE, Elshaari AW, Jöns KD, et al. Deterministic integration of single photon sources in silicon based photonic circuits. Nano Lett 2016;16:2289–94.
[211] Angelatos G, Hughes S. Theory and design of quantum light sources from quantum dots embedded in semiconductor-nanowire photonic-crystal systems. Phys Rev B 2014;90:205406.
[212] Miyazawa T, Takemoto K, Sakuma Y, et al. Single-photon generation in the 1.55-μm optical-fiber band from an InAs/InP quantum dot. Jpn J Appl Phys 2005;44:L620–2.
[213] Tumanov D, Vaish N, Nguyen HA, et al. Static strain tuning of quantum dots embedded in a photonic wire. Appl Phys Lett 2018;112:123102.
[214] Kremer PE, Dada AC, Kumar P, et al. Strain-tunable quantum dot embedded in a nanowire antenna. Phys Rev B 2014;90:201408.
[215] Fiset-Cyr A, Dalacu D, Haffouz S, et al. In-situ tuning of individual position-controlled nanowire quantum dots via laser-induced intermixing. Appl Phys Lett 2018;113:053105.
[216] van Kouwen MP, Reimer ME, Hidma AW, et al. Single electron charging in optically active nanowire quantum dots. Nano Lett 2010;10:1817–22.
[217] Reimer ME, van Kouwen MP, Hidma AW, et al. Electric field induced removal of the biexciton binding energy in a single quantum dot. Nano Lett 2011;11:645–50.
[218] Mnaymneh K, Dalacu D, McKee J, et al. Monolithic integration of single photon sources via evanescent coupling of tapered InP nanowires to SiN waveguides. arXiv:1901.00469. 2018 [arXiv preprint]. Accessed on 6 March 2019. Available at: https://arxiv.org/abs/1901.00469.
[219] Meany T, Gräfe M, Heilmann R, et al. Laser written circuits for quantum photonics. Laser Photon Rev 2015;9:363–84.